Temperature and Pressure Shaped the Evolution of Antifreeze Proteins in Polar and Deep Sea Zoarcoid Fishes

Authors: Samuel N. Bogan[1], Nathan Surendran[1], Scott Hotaling[2], Thomas Desvignes[3,4], Iliana Bista[5,6,7], Luana S.F. Lins[8], Mari H. Eilertsen[9], Nathalie R. Le François[10], Tait Algayer[11], Scott L. Hamilton[12], Paul B. Frandsen[13], Federico G. Hoffmann[14,15], and Joanna L. Kelley[1]

Affiliations:

[1] Department of Ecology and Evolutionary Biology, University of California Santa Cruz, Santa Cruz, CA USA

[2] Department of Watershed Sciences, Utah State University, Logan, UT, USA

[3] Institute of Neuroscience, University of Oregon, Eugene, OR, USA

[4] Department of Biology, University of Alabama at Birmingham, Birmingham, AL 35233, USA

[5] LOEWE Centre for Translational Biodiversity Genomics, Frankfurt, 60325, Germany

[6] Senckenberg Research Institute and Natural History Museum, Frankfurt, 60325, Germany

[7] Wellcome Sanger Institute, Tree of Life, Wellcome Genome Campus, Hinxton CB10 1SA, United Kingdom

[8] CSIRO, Health and Biosecurity, Canberra, Australia

[9] Department of Biological Sciences, Centre for Deep Sea Research, University of Bergen, Norway

[10] Laboratoire de Physiologie et Aquaculture de la Conservation (LPAC), Division des collections vivantes, de la conservation et de la recherche, Biodôme de Montréal/ Espace pour la vie, 4777, av. Pierre-De Coubertin, Montréal, Québec H1V 1B3

[11] School of Biological Sciences, Washington State University, Pullman, WA, USA

[12] Moss Landing Marine Laboratories, San Jose State University, Moss Landing, CA, USA

[13] Department of Plant and Wildlife Sciences, Brigham Young University, Provo, UT, USA

[14] Department of Biochemistry, Nutrition, and Health Promotion, Mississippi State University, Mississippi State, MS, USA

[15] Institute for Genomics, Biocomputing and Biotechnology, Mississippi State University, Mississippi State, MS, USA

Keywords: Long-read sequencing; antifreeze protein; adaptation; genomics; temperature; gene copy number

Running head: Long reads reveal antifreeze protein evolution

Abstract

Antifreeze proteins (AFPs) have enabled teleost fishes to repeatedly colonize polar seas. Four AFP types have convergently evolved in several fish lineages. AFPs inhibit ice crystal growth and lower cellular freezing point. In lineages with AFPs, species inhabiting colder environments may possess more AFP copies. Elucidating how differences in AFP copy number evolve is challenging due to the genes' tandem array structure and consequently poor resolution of these repetitive regions. Here we explore the evolution of type III AFPs (AFP III) in the globally distributed suborder Zoarcoidei, leveraging six new long-read genome assemblies. Zoarcoidei has fewer genomic resources relative to other polar fish clades while it is one of the few groups of fishes adapted to both the Arctic and Southern Oceans. Combining these new assemblies with additional long-read genomes available for Zoarcoidei, we conducted a comprehensive phylogenetic test of AFP III evolution and modeled the effects of thermal habitat and depth on AFP III gene family evolution. We confirm a single origin of AFP III via neofunctionalization of the enzyme sialic acid synthase B and show that AFP copies expanded under low temperature, but also decreased with depth, which reduces freezing point via pressure. Associations between the environment and AFP III copy number were driven by duplications of paralogs that were translocated out of the ancestral locus at which Zoarcoidei AFP arose. Our results reveal novel environmental effects on AFP evolution and demonstrate the value of high-quality genomic resources for studying how structural genomic variation shapes convergent adaptation.

65 **1. Introduction**

66 The evolution of gene family copy number variation can contribute to environmental
67 adaptation (Schmidt et al. 2010) and be stimulated by environmental change (Hull et al. 2017).
68 Studying the causes and consequences of copy number evolution is difficult when duplications
69 produce large tandem repeats or affect synteny, but the advent of long-read sequencing has helped
70 resolve repetitive variants clouding the origins of copy number evolution (Marx 2023). The
71 evolution of antifreeze proteins (AFPs) and antifreeze glycoproteins (AFGPs) are remarkable
72 examples of convergent environmental adaptation in ectotherms living at low temperatures
73 (DeVries 1971; Baskaran et al. 2021). Increased AFP 'dosage' driven by gene duplication can
74 facilitate adaptation to chronic cold (Desjardins et al. 2012). In theory, temperate species derived
75 from cold-adapted ancestors should undergo relaxed purifying selection on AFP coding regions,
76 relaxed selection on AFP copy number, and experience subsequent AFP copy number contractions
77 (Hew et al. 1988; Hayes et al. 1991). Studying contractions and expansions of AFPs across
78 thermally-distributed clades is critical for understanding thermal adaptation by ectotherms but has
79 been hampered by poor resolution of their copy number due to low quality reference genome
80 assemblies.

81 Antifreeze proteins were first discovered in Antarctic notothenioid fishes, which possess
82 antifreeze glycoproteins (AFGPs). AFGPs were found to lower both the freezing and boiling point
83 of cellular fluid (DeVries and Wohlschlag 1969; DeVries 1971; Raymond and DeVries 1977).
84 Since this discovery, AFPs that induce thermal hysteresis, an increase in degrees of difference
85 between a fluid's freezing and boiling points (Barrett 2001), have been discovered in microbes
86 (Gilbert et al. 2005), plants (Gupta and Deswal 2014), invertebrates (Duman 2015), and vertebrates
87 (DeVries and Cheng 2005). AFPs generally function by binding to the leading edges of newly-

88 crystalized nuclei of ice, attenuating their expansion and thereby reducing cellular freezing point
89 (Jia et al. 1996). In fishes, AFPs have independently evolved at least four times (Cheng and Devries
90 2002; Davies 2022). These convergently evolved AFPs make up four known categories termed
91 AFGPs, and AFP types I, II, and III. The evolution of AFPs by ectotherms is a classic example of
92 environmental adaptation, but we still know little about the environmental processes that shaped
93 their evolution and the diversity and variation they exhibit across species and their genomes.

94 It has been repeatedly suggested that, among lineages possessing AFPs, species or
95 populations inhabiting colder environments should exhibit more AFP copies (Hew et al. 1988;
96 Hayes et al. 1991; Kelley et al. 2010). Comparative studies of AFP copy number in population-
97 and species-pairs of fishes from nominally warmer versus colder habitats have confirmed this
98 expectation (Hayes et al. 1991; Desjardins et al. 2012). Prior research demonstrates that AFP genes
99 are lost in warmer, non-freezing habitats. Studying AFGPs in Arctic cod and Antarctic
100 notothenioids, Baalsrud et al. (2018) observed losses of AFGPs in secondarily sub-polar species
101 of both groups. In addition to evolving neutrally above this threshold, AFPs may be subject to
102 negative selection suggestive of costs to AFP activity. Indeed, the expression of AFPs and AFGPs
103 can disrupt organismal function through accumulation of superheated ice crystals (Celik et al.
104 2010; Cziko et al. 2014) and potentially impose costs of AFP activity in individuals experiencing
105 fluctuating freezing risk, such as many Arctic fishes (Scholander et al. 1953). Long-read
106 sequencing of notothenioids also revealed pseudogenization and contraction of AFGP copies in
107 individual species inhabiting milder latitudes suggestive of relaxed purifying selection on AFP
108 sequences or negative selection on antifreeze function (Bista et al. 2023; Rivera-Colón et al. 2023).
109 However, an analysis of AFP copy number across continuous thermal clines has not been reported.

110 Whether and how AFP copy number and gene dosage scales with freezing risk remains
111 unknown. One environmental variable that has been proposed to affect freezing risk and AFP
112 evolution is pressure. Because increased pressure in seawater affects the stability of ice crystals
113 and decreases phase change temperatures, thus lowering freezing point (Fujino et al. 1974), it has
114 been proposed that polar fishes inhabiting different depths and exhibiting divergence in AFP copy
115 number have experienced differential purifying selection or differential directional selection on
116 AFP copy number and activity (Desjardins et al. 2012). Deep ocean fishes also regulate hydrostatic
117 pressure by increasing cellular and serum osmolite content (Yancey et al. 2002; Yancey et al.
118 2014), which may further reduce internal organismal freezing temperatures.

119 AFPs of bony fishes have evolved by neofunctionalization, and AFGPs by both
120 neofunctionalization and *de novo* gene birth. These events were driven in part by repetitive
121 genomic regions that provided substrate for *de novo* gene birth of an AFGP in cods (Baalsrud et
122 al. 2018; Zhuang et al. 2019) and AFP I flounder (Rives et al. 2024). AFP III evolved in Zoarcoidei
123 fishes via translocation of ancestral genes that underwent neofunctionalization and expanded into
124 tandem arrays of AFPs (Deng et al. 2010; Hotaling et al. 2023). AFP I also evolved via
125 neofunctionalization in sculpins (Graham and Davies 2024). In addition to influencing AFP
126 origins, structural variation such as translocations, inversions, and repetitive element content have
127 the potential to influence expansions and contractions of AFPs across environmental gradients
128 (Lauer and Gresham 2019). For example, cytogenetically-balanced and unbalanced translocations
129 can both facilitate variation in gene copy number (Watson et al. 2007; Harewood et al. 2010). The
130 accurate detection of translocations and measurement of gene copy number in repetitive regions
131 require long-read sequencing approaches, which enable identification of structural variants such
132 as translocations and better resolve complex genomic regions relative to short read sequencing

133 (Marx 2023). Long-read sequencing has shown success in assembling repetitive AFGP arrays in
134 notothenioid fishes (Bista et al. 2023; Rivera-Colón et al. 2023)

135 The bony fish suborder Zoarcoidei is an ideal system in which to study the joint effects of
136 environmental and structural genomic variation on AFP evolution. Zoarcoidei likely originated in
137 north temperate seas, followed by stepwise invasions of (i) the Arctic Ocean, (ii) south temperate
138 seas and (iii) the Southern Ocean (Anderson 1994; Radchenko 2016; Hobbs et al. 2020; Hotaling
139 et al. 2021) where minimum temperatures can fall below -2.0 °C (Fetterer 2017; Auger et al. 2021).
140 Multiple deep sea environments exhibit temperatures below 0 °C and as low as -2.0 °C (Ponte
141 2013). These extremely low temperatures can cause freezing in tissues and serum (Storey and
142 Storey 1988) and the formation of sea ice at ocean surfaces and as brinicles within the water
143 column (Worster and Rees Jones 2015). Fish tissues typically possess higher freezing points than
144 seawater as they are hypoosmotic to their environment (Hargens 1972), posing freezing risk even
145 in the absence of sea ice. Sanger sequencing of BAC clones in the zoarcoid *Lycodichthys dearborni*
146 suggested that type III AFP arose within Zoarcoidei via neofunctionalization of the enzyme sialic
147 acid synthase B (*sasb*) (Deng et al. 2010). *sasb* likely duplicated before undergoing deletions of
148 all exons except 1 and 6, which are homologous to AFP III exons 1 and 2 (Deng et al. 2010).
149 Zoarcoidei repeatedly invaded and adapted to the poles (Hotaling et al. 2021) while Zoarcoidei
150 AFP III likely evolved once (Deng et al. 2010; Hobbs et al. 2020).

151 AFP III copies have likely expanded and contracted multiple times in Zoarcoidei (Hotaling
152 et al. 2023), but the extent of gene family evolution of AFP III in zoarcoids, of AFPs across fishes,
153 and how genomic and environmental variation interactively affected AFP evolution remain
154 unclear. Zoarcoidei diversified across depth faster than any group of fishes (Friedman and Muñoz
155 2023), potentiating a complex landscape of selection for AFP function and dosage across the

156 suborder's distributions through latitude and depth. Previously identified tandem arrays of
157 zoarcoid AFP III exhibited conserved synteny with several flanking genes (Hotaling et al. 2023),
158 enabling identification of translocations out of this region.

159 Here we report high-quality, long-read genome assemblies from six species of Zoarcoidei
160 from diverse thermal habitats and depths (Fig. 1; Table 1). We integrated annotations of AFP III
161 genes with oceanographic measures of thermal minima, pressure, and depth within species'
162 habitats to test the hypothesis that temperature and pressure are associated with AFP III copy
163 number evolution. We predict that AFP copies contracted in deep ocean, higher-temperature
164 species through relaxed purifying selection or negative directional selection on AFP function and
165 copy number. Using analyses of synteny, we traced AFP III copies to ancestral and translocated
166 arrays and determined whether translocation drove AFP expansions under high freezing risk.
167 These new reference genome assemblies provide a valuable resource for studying how abiotic
168 environments and structural variation jointly influence convergent adaptation.

169

170 **2. Results and Discussion**

171 *2.1. Genome assembly* - Reference genomes were assembled with Pacific Biosciences
172 (PacBio) long-read sequence data for six zoarcoid fishes spanning a range of temperatures and
173 depths: the ronquil *Bathymaster signatus*, the wolffishes *Anarhichas lupus* and *Anarhichas minor*,
174 and the eelpouts *Lycenchelys platyrhina*, *Lycodes diapterus*, and *Ophthalmolycus amberensis*.
175 These species inhabit polar seas with latitudes as northerly as 73.0 °N and southerly as -65.8 °S.
176 Assembled genomes included temperate species with absolute latitudes as low as 37.8 ° (Fig. 1).
177 Species' maximum depths spanned 24 - 2,229 meters. These mark the first long-read genome
178 assemblies for the families Bathymasteridae (ronquils) and Anarhichadidae (wolffishes), and

179 increase the number of long-read genome assemblies among Zoarcidae (eelpouts) by two and a
180 half times.

181 Genome sizes, sequencing coverage, N50 values, BUSCO complete percentages, and
182 percent repetitive elements are reported in Table 1 for the six new assemblies, five existing
183 zoarcoid long-read assemblies (Rhie et al. 2021; Programme et al. 2022; Wright et al. 2023; Bista
184 et al. 2024), and one scorpaeniform outgroup (Nath et al. 2021). Genome sizes of all Zoarcoidei
185 examined equaled a mean of 647.80 ± 74.3 Mb. Genome assemblies reported here averaged 11.7x
186 greater coverage compared to publicly available, long-read zoarcoid assemblies. Contig N50
187 values were an average of 6.5 Mb longer than available assemblies (Table 1). As expected,
188 repetitive element content linearly and positively correlated with genome size across all species
189 (Kidwell 2002) as shown in Fig. S1 ($r^2 = 0.93$).

190 Zoarcoidei families are among the few fish groups inhabiting both the Arctic and Southern
191 Oceans (Møller et al. 2005), positioning this suborder to be a valuable system in which to study
192 convergent evolution and adaptation to extreme cold. However, a paucity of genomic resources
193 for zoarcoid fishes stands as an obstacle to their value in research. The improved reference genome
194 quality of these new assemblies among other members of Zoarcoidei and the extension of thermal
195 habitats and depths represented among them significantly strengthen Zoarcoidei as a tractable,
196 valuable system in which to study convergent adaptation.

197 *2.2. Variation in type III antifreeze protein copy number* - The number of AFP III copies
198 in the 11 zoarcoids studied ranged from 0 to 42 putatively functional copies. Between 3 and 16
199 pseudogenized AFP III copies were detected across all zoarcoids (Fig. 1A). The copy number of
200

201 **Table 1 |** *Genome assembly metrics.* Genomes include those reported by the authors in this study (rows 1-
202 5) and Hotaling et al. 2023 (row 6). Assemblies reported by the authors are shaded in gray. Publicly
203 available zoarcoid genomes leveraged in this study are not highlighted. A non-zoarcoid outgroup is
204 designated by an asterisk. BUSCO analysis was performed on universal single-copy orthologs of
205 Actinopterygii.
206

Species	Genome size (Mb)	Sequence coverage	Contig N50 (Mb)	Scaffold N50 (Mb)	% Repetitive elements	BUSCO % complete (*n* orthologs)	NCBI accession/ BioProject
Anarhichas lupus	627.7	80x	23.8	*na*	27.0%	98.5% (3587)	PRJNA980960
Anarhichas minor	643.9	74x	13.2	*na*	28.0%	98.5% (3587)	PRJNA982125
Bathymaster signatus	714.3	42x	3.1	*na*	32.2%	98.3% (3587)	PRJNA982427
Lycodes diapterus	711.9	43x	6.0	*na*	34.1%	98.5% (3585)	PRJNA982746
Lycenchelys platyrhina	718.5	34x	2.8	*na*	31.0%	98.3% (3579)	PRJNA985917
Ophthalmolycus amberensis	712.6	95x	5.8	*na*	30.6%	98.5% (3586)	PRJNA701078
Cebidichthys violaceus	575.7	31x	1.0	16.4	25.4%	93.3% (3396)	GCA_023349555.1
*Gasterosteus aculeatus**	471.9	75x	0.5	20.5	18.6%	97.0% (3534)	GCA_016920845.1
Leptoclinus maculatus	699.9	65x	2.4	23.5	32.8%	98.0% (3569)	GCA_032191485.1
Lycodes pacificus	646.4	68x	4.7	27.7	29.0%	98.1% (3573)	GCA_028022725.1
Melanostigma gelatinosum	662.0	39x	1.9	28.0	29.3%	98.1% (3569)	GCA_949748355.1
Pholis gunnellus	588.7	45x	3.5	25.4	23.3%	98.6% (3591)	GCA_910591455.2

207 putatively-functional and pseudogenized AFP genes correlated such that pseudogenes increased
208 in species with more AFP III copies (Fig. S2; $r^2 = 0.31$). This association was explained by

209 phylogeny and became insignificant after controlling for species relatedness (95% posterior
210 interval = -1.54 – 0.67). The presence of pseudogenized AFP III copies in all zoarcoids indicates
211 that the gene's origin predates the most-recent common ancestor of zoarcoids included in this study
212 (Fig. 1A). From here forward, all results correspond to the study of putatively functional AFP
213 copies and do not include pseudogenes.

214 We evaluated whether AFP III may have arisen in a common ancestor predating Zoarcoidei
215 by screening for the gene in long-read assemblies of 12 species of the Order Scorpaeniformes,
216 representing 7 families, and found no evidence of complete or partial AFP III paralogs (Table S2).
217 Past phylogenetic analyses of zoarcoid AFP III also detected a partial, pseudogenized AFP III
218 sequence in Bathymasteridae, the earliest-branching family of Zoarcoidei (Hobbs et al. 2020).
219 However, Hobbs et al. (2020) and others have not ruled out an emergence of AFP III prior to the
220 branching of Zoarcoidei. Our results therefore strengthen evidence that Zoarcoidei AFP III likely
221 arose in a common ancestor Bathymasteridae and Zoarcoidei as opposed to a common ancestor
222 within Scorpaeniformes predating Zoarcoidei. Long-read sequencing of Zoarcoidei offers the
223 potential to trace the origin of AFP III within Zoarcoidei by mapping structural variants
224 contributing to the gene's evolution. These events include duplication-translocation of *sasb* and
225 deletions of *sasb* exons 2 – 5.

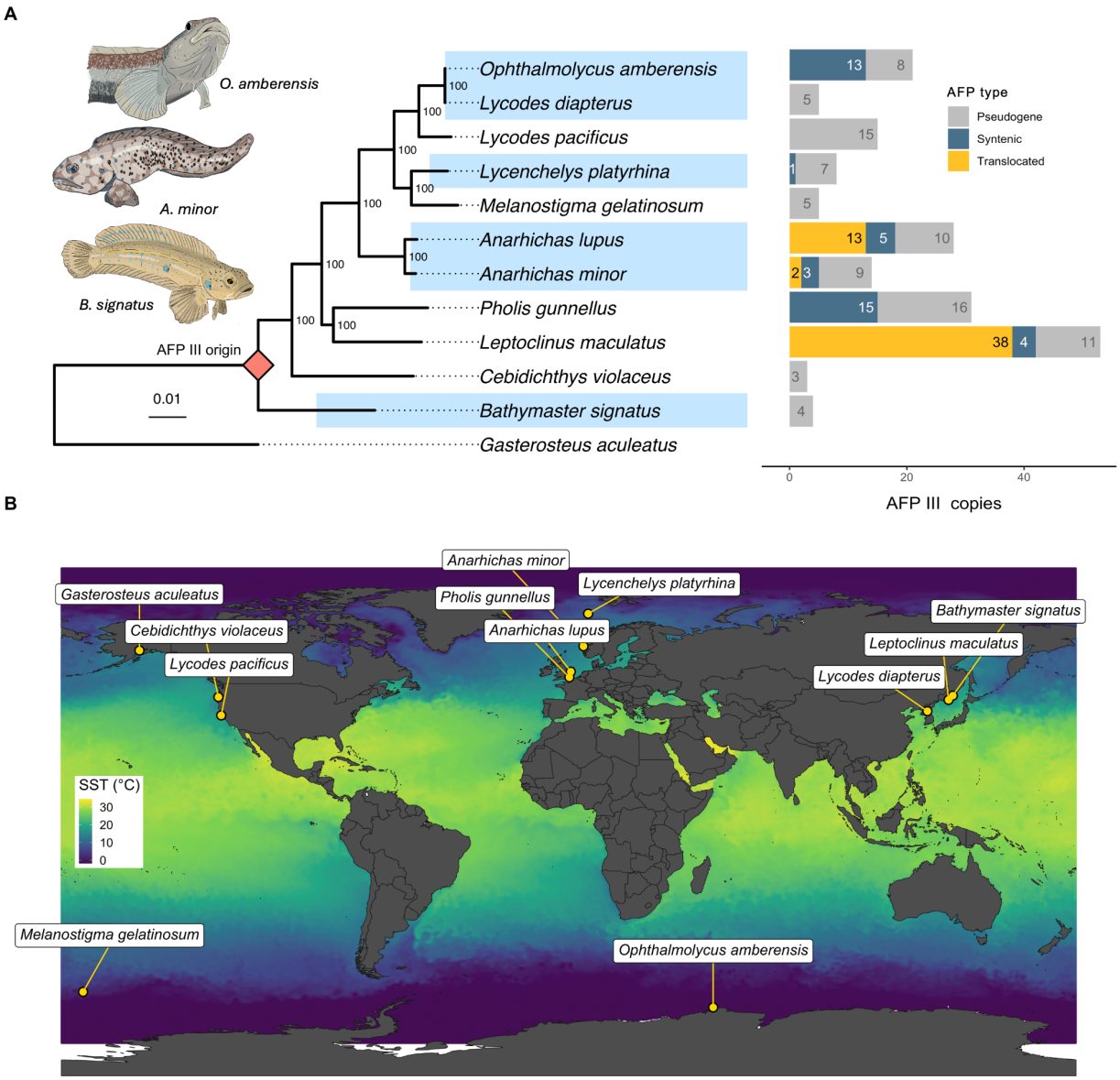

Figure 1 | *Species' phylogeny, AFP copy numbers, and distributions.* (A) A species tree of Zoarcoidei included in this study including outgroup *Gasterosteus aculeatus* is plotted adjacent to AFP copy number variation colored by pseudogenization or location of homologs in the ancestral syntenic region or translocation(s). The red diamond signifies the origin of type III AFP. Nodes are labeled with bootstrapped support values. Species highlighted in blue denote genome assemblies reported by the authors in this study and Hotaling et al. (2023). The scale bar denotes substitutions per amino acid. *Ophthalmolycus amberensis* and *Lycodes diapterus* branch tip lengths equal 0.000069 and 0.000074 substitutions per amino acid, respectively. (B) Species' distributions are plotted as the point of maximum likelihood of occurrence from AquaMaps standardized distributions. The size of white circles around occurrences are scaled according to species abundance. Mean sea surface temperature (SST, °C) recorded in August, 2020, is visualized according to color. Illustrations by SNB.

239 *2.3. Environmental effects on type III antifreeze protein copy number* - Habitat temperature
240 and pressure jointly influence freezing risk (Fujino et al. 1974) and were additively correlated with
241 AFP copy number such that AFP copy number expanded in shallow, cold-water species (Fig. 2A).
242 A phylogenetically corrected Bayesian model revealed that AFP copy number significantly
243 increased with decreases in (i) thermal minima of species' habitats and (ii) mean pressure of
244 species' depth ranges (Fig. 2). Thermal minima equaled the lowest recorded temperature at a
245 species' coordinate of maximum likelihood of occurrence within their depth range. Pressure was
246 derived from habitat depth and latitude. Thermal minima of species habitats spanned -3.00 to 7.21
247 °C (Fig. S3). AFP copy number significantly increased in species occupying lower thermal minima
248 (Fig. 2B). This effect was significant after controlling for phylogeny (scaled effect = -1.55 ± 0.97).
249 It is possible that a thermal gradient in AFP III copy number evolved in Zoarcoidei via mutation
250 that preceded and enabled invasion of novel temperatures or changes in copy number that followed
251 the invasion of new temperatures inducing selective pressure.
252

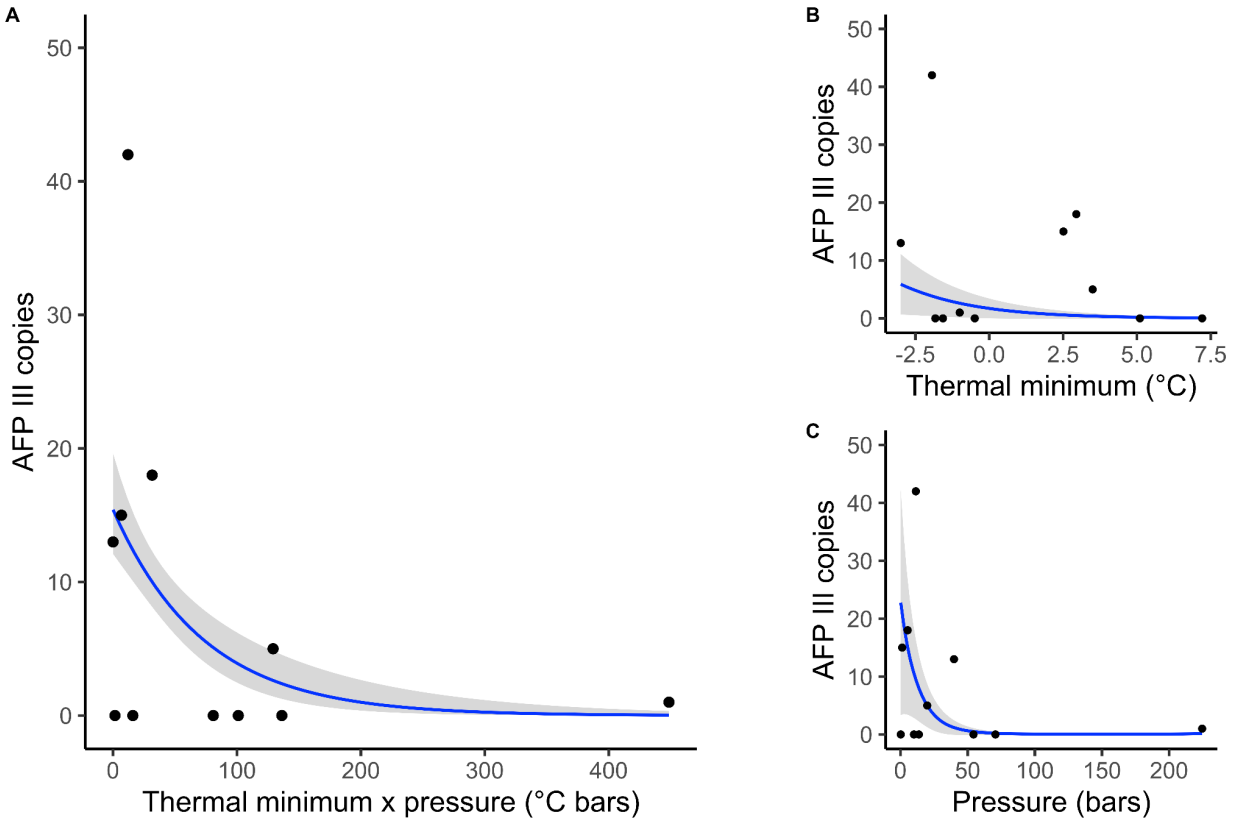

Figure 2 | *Associations between temperature, pressure, and type III antifreeze protein copy number.* (A) AFP expansions in shallow, cold-water species are visualized as a logistic regression of AFP copy number fitted to the product of mean habitat pressure and habitat thermal minimum, with the lowest thermal minimum scaled to 0. Panels on the right show relationships between AFP III copy number and (B) thermal minima of species habitats and (C) mean pressure of species' habitats are plotted. Fitted lines represent fit from a phylogenetically controlled model of type III antifreeze protein copy number.

AFP III gene copy number declined in species inhabiting greater pressure (Fig. 2C). Pressure had a stronger effect on AFP copy number than temperature and was non-linear, following a negative exponential curve. Pressure, which varies as a function of depth and latitude, affected AFP copy number after controlling for habitat depth as well as phylogeny (scaled linear effect = -4.72 ± 2.58). This suggests that pressure, rather than depth, predicted AFP copy number. Habitat temperatures correlated with depth and pressure (Fig. S4 – S5). To account for this autocorrelation, predicted effects of thermal minima and pressure on AFP copy number were modeled in a statistically independent manner. The finding that AFP III copy number is reduced

269 in deep sea species experiencing high pressure is pertinent to the biogeography of Zoarcoidei,
270 which includes the eelpout family Zoarcidae that has exhibited faster rates of evolution across
271 depth than any group of fishes (Friedman and Muñoz 2023). Associations between depth and AFP
272 copy number were previously proposed by Desjardins et al. 2012, who observed that the wolffishes
273 *A. lupus* and *A. minor* exhibit higher AFP copy number in the shallow water species *A. lupus* rather
274 than *A. minor* the species occupying a colder thermal environment (Desjardins et al. 2012). Our
275 results mark the first quantitative evidence that selection on antifreeze proteins across thermal
276 environments was shaped by pressure.

277 A direct explanation of the association between pressure and AFP copy number is that
278 increased energy imposed by pressure lowers the freezing point of intracellular fluids (Fujino et
279 al. 1974). An indirect explanation also exists that is not mutually exclusive to this direct hypothesis.
280 Deep sea fishes generally regulate the hydrostatic pressure of cells through osmoregulation, such
281 that increased pressure is countered by greater osmolarity in cells and serum, where AFPs are
282 secreted (Griffith 1981; Gillett et al. 1997; Yancey et al. 2002; Yancey et al. 2014). Because
283 increased osmolality also reduces the freezing point of fluids (Potter et al. 1978; Bodnar 1993), it
284 pressure and osmolality may have additively affected freezing point.

285 It is possible that reductions in AFP gene copy number in species of warmer minimum
286 habitat temperature can be attributed to relaxed purifying selection on AFP sequence and/or
287 negative selection on AFP copy number or AFP function. Many polar fishes inhabiting the Arctic
288 Ocean and almost all polar fishes included in our study, excluding *O. amberensis,* experience
289 temporal and spatial variation in freezing risk across their range and throughout the year (Reist et
290 al. 2006; Verde et al. 2006). It is likely that fishes which have expressed AFPs to attenuate ice
291 growth under freezing conditions incur a cost to AFP function during episodic non-freezing

292 conditions. Fishes that experience more frequent temperatures above freezing point may
293 experience stronger negative selection on AFP expression level or function, which would select
294 for reduced copy number and/or AFP activity. Additionally, some non-polar populations share
295 connectivity with polar populations experiencing freezing risk (Hickerson and Cunningham 2006)
296 and populations that do not experience freezing risk may possess allele frequencies that have been
297 shaped by selection on AFP sequence or function in connected, polar populations.

298 *2.4. Gene family evolution and convergence of antifreeze protein copy number* - Restricted
299 maximum likelihood ancestral state reconstruction of AFP III copy number demonstrated that at
300 least 8 expansions and 12 contractions of AFP III occurred across the studied phylogeny (Fig. S6).
301 To evaluate whether AFP contractions and expansions convergently evolved during independent
302 invasions of polar or deep seas, the phylogenetically-controlled model of environmental
303 associations with AFP III copy number was expanded as a structural equation model predicting
304 both habitat thermal minima and mean pressure as a function of phylogenetic relatedness. This
305 enabled regression of AFP III copy number against phylogenetically-independent invasions of
306 colder or higher-pressure environments, which is necessary for quantifying convergence.
307 Independent invasions of lower thermal minima were significantly associated with increased AFP
308 III copy number (95% posterior interval = -1.15 – -0.03 AFP copies per °C). Phylogenetically-
309 independent changes in habitat thermal minima and AFP copy number are plotted in Figures S7-
310 8. Despite having a stronger association with pressure before testing for convergence, independent
311 invasions of higher pressure habitats were not associated with decreased AFP III copy number.

312 While the association between AFP III copy number and habitat pressure among extant
313 branches was stronger than with thermal minimum, there is little evidence that this association
314 resulted from convergent evolution between independent invasions of the deep ocean. By contrast,

315 weaker associations between temperature and AFP III are more likely to have evolved as a result
316 of convergent gains and losses of AFP III during invasions of Zoarcoidei into colder and warmer
317 environments, respectively. The pole-to-pole distribution of Zoarcoidei is marked by a likely
318 origin in the Arctic followed by invasion of the deep ocean, trans-polar migration across deep-
319 ocean regions, and subsequent reinvasion of shallow waters in the Southern Ocean (Hobbs et al.
320 2020; Hotaling et al. 2023). The ancestral state reconstruction of thermal minima shows repeated
321 invasions of sub-zero oceans across Zoarcoidei (Fig. S7). As shown in Figure S9, the
322 reconstruction of habitat pressure shows one primary lineage of deep ocean fishes belonging to the
323 eelpout family Zoarcidae, which is the deepest dwelling family of zoarcoid fishes. Thus, the strong
324 effect of pressure on AFP III copies across Zoarcoidei was more likely attributed to a singular
325 invasion of the deep sea by Zoarcidae rather than multiple convergent events. Decreases in habitat
326 pressure in Zoarcidae that corresponded with increased AFP III copy number represent instances
327 of parallel rather than convergent evolution. Phylogenetically-independent changes in habitat
328 pressure and AFP copy number are plotted in Figures S9-10.

329 Using maximum likelihood gene tree inference, we confirmed the origin of AFP III
330 evolution in Zoarcoidei. Our tree of all *sasa*, *sasb*, and AFP III homologs across study species is
331 consistent with a single origin of AFP III from *sasb* (Deng et al. 2010) as shown in Figure 3C.
332 However, the topology of the gene tree does not provide evidence of whether the common ancestor
333 of Zoarcoidei arose at the syntenically-conserved array or translocated locus. For the gene tree to
334 illuminate the positional origin of Zoarcoidei AFP, a monophyletic cluster of syntenic or
335 translocated AFPs would have to be the first lineage to diverge from all other AFPs. The gene tree
336 does not show a monophyletic cluster of translocated AFPs as the first diverging group of
337 Zoarcoidei AFP. Therefore, maximum likelihood ancestral state reconstructions were used to

338 predict binary characters of whether species possessed AFP III in the syntenic locus or in one of
339 the six translocated loci. These reconstructions demonstrated that ancestral Zoarcoidei AFP III
340 most likely arose in the syntenic region rather than one of the translocated positions (relative
341 likelihood = 727.89 – 1440.39).

342 *2.5. Role of translocation in AFP III expansions* - The ancestral AFP III array falls within
343 a conserved, syntenic region flanked by genes including synuclein gamma (*sncgb*) and LIM-
344 binding domain protein (*ldb3b*) as previously shown by Deng et al. (2010). We identified at least
345 six independent translocations of AFP III out of the ancestral syntenic region (Fig. 3B). All
346 zoarcoids with AFP III retained this microsynteny, such that at least some AFP III copies were
347 flanked upstream by *sncgb* and downstream by *ldb3b* (Fig. 3A). Whole-contig alignment revealed
348 conservation of synteny across larger genomic scales. The ancestral AFP III tandem repeat region,
349 flanked by *sncgb* and *ldb3b*, fell in the same homologous region of chromosome 21 across
350 Zoarcoidei (Fig. 3B). In *L. maculatus*, however, the ancestral AFP III array was positioned in a ~3
351 Mb chromosomal inversion (Fig. 3B). Translocated AFPs clustered into three gene clades (Fig.
352 3C). In *P. gunnellus*, one AFP copy on chromosome 21 fell outside of the flanking genes *sncgb*
353 and *ldb3b* (Fig. 3A).

354 AFP III copies outside of the ancestral array mapped to two translocated regions in each of
355 three species, totalling six translocated arrays across all study species. The wolffishes *A. lupus* and
356 *A. minor* each contained two translocations on contigs homologous to *P. gunnellus* chromosome
357 2. However, the two translocated arrays in *A. lupus* and the two in *A. minor*
358

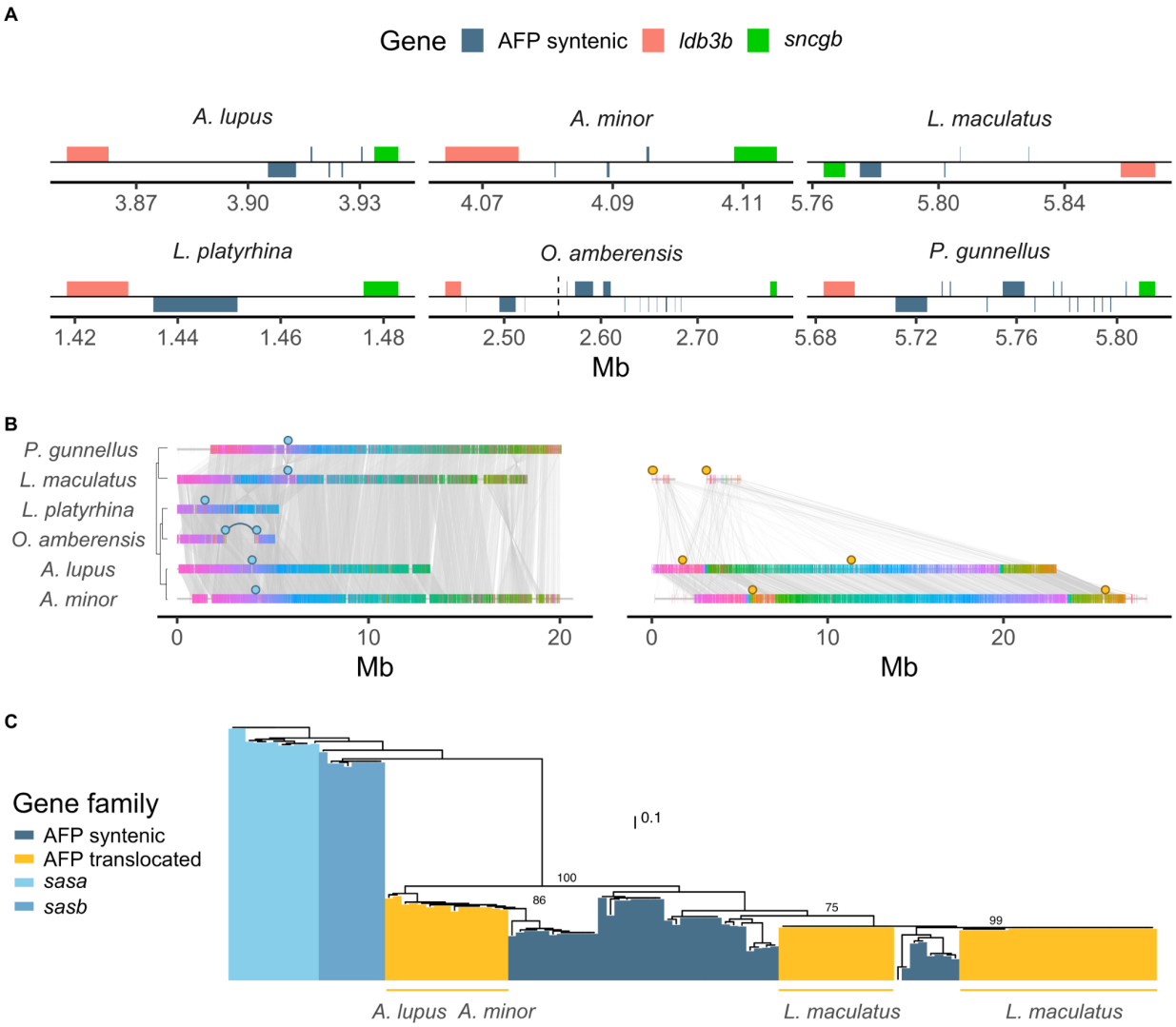

Figure 3 | *Synteny and origin of type III antifreeze proteins.* (A) Microsynteny at the ancestral, syntenic Zoarcoidei AFP array is visualized by annotation tracks colored by whether they represent AFPs or genes flanking the array (*ldb3b* and *sncgb*). The vertical dashed line in *O. amberensis* represents a junction between contig fragments. Tracks represent the full lengths of gene exons and introns. (B) Synteny of AFP III tandem arrays. Full lengths of scaffolds and contigs are shown. Colored bars represent regions conserved in at least two species. Regions sharing the same color are homologous. Gray lines connect these homologous regions. Narrow horizontal bars depict regions lacking homology. Positions of ancestral, syntenic AFP arrays are marked by blue circles and translocated arrays by orange circles. Curved lines connect single AFP arrays split between contigs. A species distance tree is inset into the left hand side of the syntenic array panel. (C) A rooted gene tree of *sasa*, *sasb* and AFP III paralogs. Branches are colored by syntenic AFPs, translocated AFPs, *sasa*, or *sasb* genes. The scale bar represents nucleotide substitutions per base pair. Bootstrap support values are included to the right of all nodes that branch into clades of syntenic and translocated AFPs. The taxonomic groups that translocated AFPs belong to are annotated below translocated AFP clades. The node most closely related to *sasb* branches into gene clades of translocated and syntenic AFPs, prohibiting resolution of whether ancestral Zoarcoidei AFP evolved in the syntenically conserved region. Tests of whether Zoaroidei AFP arose in the syntenic region are described under '*Gene family evolution and convergence of antifreeze protein copy number*'.

377 possessed differing synteny, falling into four distinctly different regions of chromosome 2 (Fig.
378 3B). Thus, these arrays likely represent four discrete translocation-duplication events. The two
379 translocated arrays in *L. maculatus* were distributed across two contigs mapping to different
380 regions of *P. gunnellus* chromosome 12 (Fig. 3B). Translocated copies contributed significantly
381 to AFP III expansions across Zoarcoidei, making up 13 of 18 (72%) AFP copies in *A. lupus*, 2 of
382 5 (40%) copies in *A. minor*, and 38 of 42 (90%) copies in *L. maculatus* (Fig. 1A). Considering the
383 short lengths of contigs in which translocated AFP III were located *L. maculatus* (Fig. 3B), there
384 is potential for misassembly to have inflated the total number of translocations, the AFP copy
385 number within translocated arrays, and the total AFP copy number in this species. Conversely,
386 translocated arrays that border the ends of these contigs may also cause underreporting of total
387 AFP copy number at these locations (Fig. 3B).

388 A multivariate phylogenetic model predicting syntenic and translocated AFP III copy
389 number as a function of thermal minima and pressure revealed that environmental gradients in
390 AFP copy number were driven by expansions of translocated homologs. After controlling for
391 phylogeny, habitat thermal minima was associated with syntenic AFP copies at a scaled effect
392 strength of -0.62 ± 0.72 and translocated AFP copies at -1.36 ± 0.70 (Fig. 4A). Mean habitat
393 pressure yielded an effect on syntenic copies of -0.88 ± 0.54 and an effect on translocated copies
394 of -9.84 ± 3.08 (Fig. 4B).

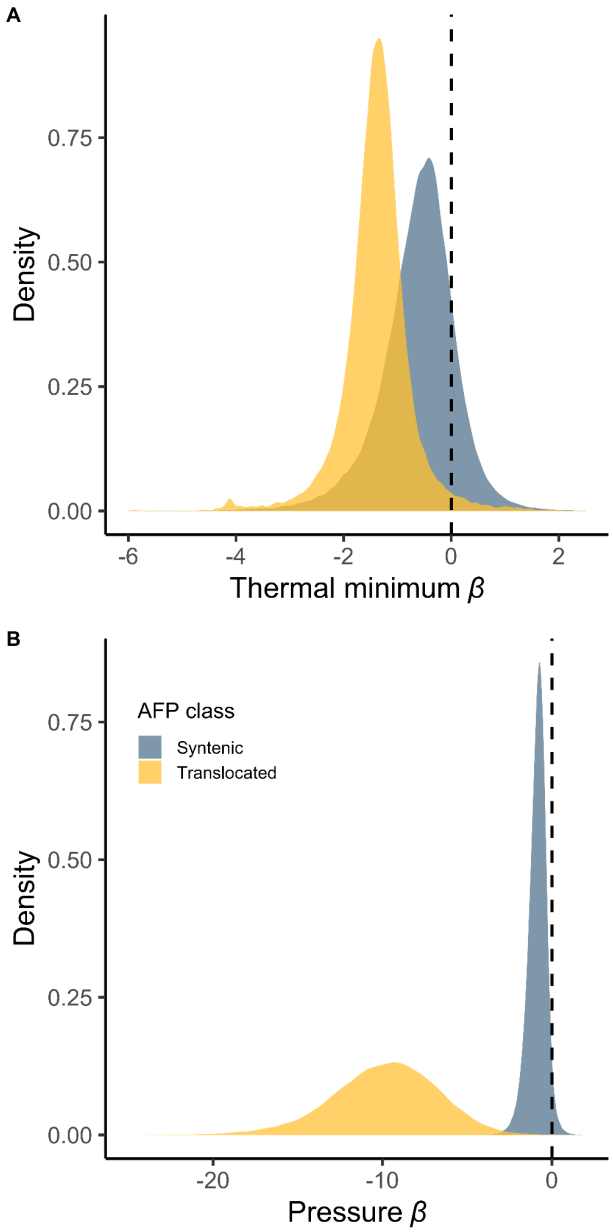

Figure 4 | *Effects of thermal minimum and pressure on copy number of syntenicically-conserved and translocated type III antifreeze protein genes*. Densities represent the posterior probabilities for fixed effects (β) of (A) thermal minimum and (B) mean pressure on antifreeze protein copy in ancestral, syntenically-conserved versus translocated sites.

Molecular repair mechanisms causing variation in copy number such as break-induced replication can directly facilitate translocation of gene copies to regions sharing microhomology with break sites (Hastings, Lupski, et al. 2009; Hastings, Ira, et al. 2009; Kramara et al. 2018). It

405 is possible that expansions of AFP III via translocation are simply a consequence of selection for
406 high copy number. AFP III translocations were not more likely among species with a large number
407 of AFPs, however. Rather, copy number in translocated arrays correlated with habitat temperature
408 and pressure. This is suggestive of directional selection acting more strongly on AFP copy number
409 outside of the syntenic, ancestral AFP III locus. Differences in directional selection on copies may
410 arise as a consequence of subfunctionalization stemming from transcriptional changes that occur
411 following translocation into new regulatory landscapes (Harewood et al. 2010; Wang et al. 2012).
412 Alternatively, copy number at the ancestral AFP array may be under stronger stabilizing selection
413 and evolutionary constraint relative to translocated arrays.

414 Bayesian Ornstein-Uhlenbeck phylogenetic mixed models were used to evaluate copy
415 number of syntenic and translocated AFPs across the Zoarcoidei tree. We observed 7.03x greater
416 stabilizing selection (α) on syntenic copy number relative to translocations. Differences in
417 selection were significant as evidenced by a Bayes factor test of α posterior probabilities yielding
418 BF = 41.77 (Fig. 5A). Purifying and diversifying selection on coding sequences were modeled
419 across the AFP III gene tree using branch-tip estimates of d_N/d_S. Syntenic and translocated AFPs
420 were both under strong purifying selection, demonstrating that translocated AFPs remain
421 evolutionarily conserved. Translocated AFPs exhibited lower d_N/d_S ratios than syntenic copies, but
422 this difference was insignificant. Genes with longer branch lengths had significantly higher d_N/d_S
423 ratios on average as shown in Figure 5B (scaled posterior interval = 0.17 – 0.89). It is possible that
424 translocated AFPs exhibited stronger purifying selection in our test, not because they have truly
425 been under stronger purifying selection, but because of an analytical artifact that stems from having
426 duplicated more recently.
427

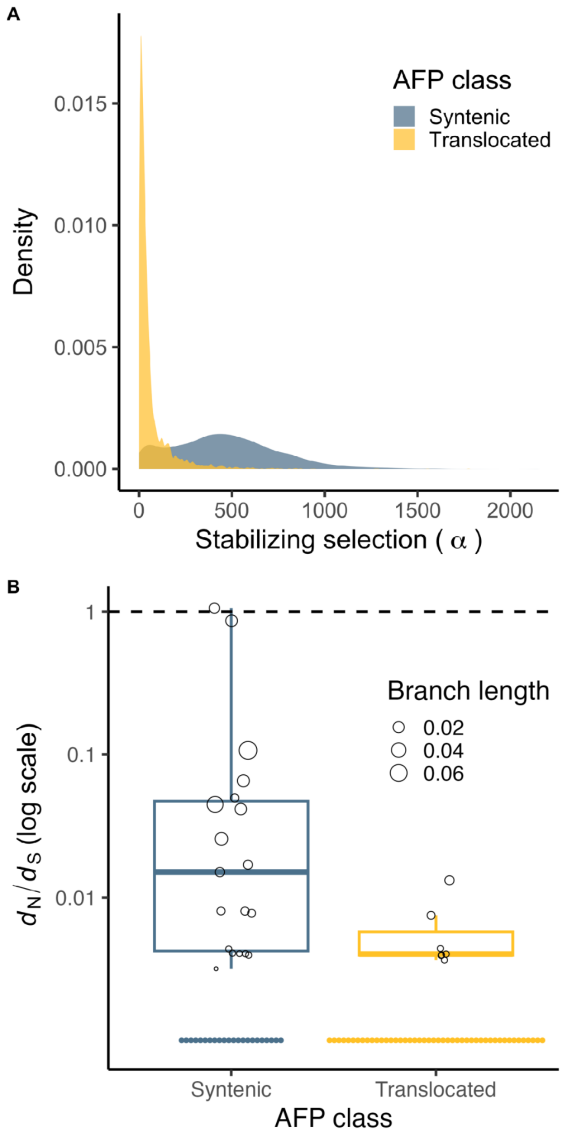

Figure 5 | *Selection on type III antifreeze protein (AFP) copy number and coding sequence*. (A) Posterior probabilities of stabilizing selection (α) on copy number of syntenic and translocated AFP III homologs across the Zoarcoidei tree derived from an Ornstein-Uhlenbeck phylogenetic mixed model. (B) Branch-tip d_N/d_S ratios specific to syntenic and translocated AFP III homologs modeled in HyPhy RELAX. Each point represents a single gene. Branch length is depicted by point size. d_N/d_S ratios of branch tips that lacked substitutions were undetermined and visualized below 0 as solid black circles.

Studies observing environmental effects on gene copy number are abundant (Kondrashov 2012; Lauer and Gresham 2019; Mérot et al. 2020), but the role of translocation in mediating environmental gradients of copy number is less understood. In populations of salmon, a chromosomal translocation shows strong genotype-environment association with temperature

(Watson et al. 2022) while in soybean, a reciprocal chromosomal translocation may have facilitated climatic adaptation (Wang et al. 2021). Furthermore, translocation duplications of AFGP have been observed in notothenioid icefishes (Rivera-Colón et al. 2023), indicating potential for translocation to affect environmental gradients of antifreeze gene copy number in other systems. Our results expand on these studies by demonstrating that not only translocation, but its association with copy number, can contribute to molecular evolution across environments.

While our approach evaluated the hypothesis that AFPs expanded in shallow, polar zoarcoid species at a macroevolutionary scale, it is likely that environmental gradients in AFP copy number were attributed to intraspecific evolution as well. Population genomic studies of AFP III structural variation within Zoarcoidei species are necessary for further understanding environmental gradients in AFP copy number and the potential role of translocation in shaping these gradients. Intraspecific AFP copy number variation has been observed in populations of winter flounder inhabiting different depths and extents of sea ice cover (Hayes et al. 1991). Zoarcoids included in our study inhabit ranges that, in some cases, span both non-freezing and freezing conditions. Neutral and adaptive variation shaping AFP III copy number across the Zoarcoidei suborder can be more finely resolved by resequencing of conspecifics and populations distributed across gradients of temperature, pressure, and freezing risk. Detection and modeling of adaptive and neutral variation in AFP copy number is necessary for evaluating (i) additional evidence of whether copy number-environment associations arose via drift and (ii) whether non-neutral copy number variation is greater among translocated AFP III arrays.

462 **3. Conclusion**

463 Structural variation observable via long-read sequencing appears to have been critical for
464 AFP III gene family evolution during the convergent adaptation of Zoarcoidei to both poles. Our
465 findings highlight the role of multiple environmental stressors (temperature and pressure) in
466 shaping the genetic architecture of adaptations like antifreeze function. Furthermore, structural
467 variants such as translocations may act as gatekeepers of adaptation by constraining or facilitating
468 molecular evolution under the selective pressures of those stressors. Future research should address
469 whether translocation-associated gene family expansions are driven by mechanisms associated
470 with transposable element architecture at translocation endpoints or break-induced replication. The
471 reported, long-read Zoarcoidei reference genomes offer further potential to study the role of
472 structural variation and chromosomal translocation in convergent environmental adaptation, as
473 well as the complex evolution of antifreeze proteins.

474

475 **4. Materials and Methods**

476 *4.1. DNA extraction, sequencing, and genome assembly* - *Lycenchelys platyrhina* was
477 collected from the Norwegian Sea, Ægir vent field, Norway (72.3286 °N, 1.5178 °E) on July 28th,
478 2021. The specimen for *Lycenchelys platyrhina* (originally described as *Lycodes platyrhinus*
479 Jensen, 1902) received a putative identification during collection which required genomic
480 identification and statistical consideration. *L. platyrhina* is a rarely observed species associated
481 with only 11 occurrences in the Global Biodiversity Information Facility. The sequenced specimen
482 was collected inside the range of *L. platyrhina* observations (67.1 - 73.8 °N, 10.3 °W - 8.2 °E). To
483 this end, mitochondrial scaffolds of the *L. platyrhina* assembly were aligned to the NCBI
484 nucleotide database using blastn (Altschul et al. 1990). No sequence of *Lycenchelys platyrhina*

485 was available in the database. The top 10 greatest percent similarity blast hits were with species of
486 the family Lycodinae to which *L. platyrhina* belongs; top 5 = *O. amberensis* (95.88%) *Lycenchelys*
487 *kolthoffi* (95.57%), *Lycenchelys raridens* (95.05%), *Lycenchelys muraena* (94.60%), and
488 *Lycenchelys sarsii* (94.60%). Skeletal muscle from a single individual was used for DNA isolation
489 using the Circulomics Nanobind, BIG DNA prep, Tissue protocol. Isolated genomic DNA was
490 quantified with a Fragment Analyzer (Agilent). Ampure-PB beads were used to purify and remove
491 short fragments from the sample prior to library prep according to manufacturer protocol. A second
492 size selection for >10 kb fragments was performed on the sample using a BluePippin system (Sage
493 Science Inc., Beverly, MA, USA) with a 10kb cutoff. A library was prepared without shearing
494 using SMRTbell® ExpressTemplate Prep Kit 3.0. Final library was size selected using BluePippin
495 with an 8 kb cutoff. The library was sequenced on one 8M SMRT cells on Sequel IIe instrument
496 using Sequel II Binding kit 2.2 and Sequencing Chemistry v2.0. Loading was performed by
497 adaptive loading, movie time: 30 hours, pre-extension 2 hours.

498 Sampling of *Anarhichas lupus* was performed in July, 2022, on a captive-reared individual
499 derived from eggs collected in Conception Bay, Newfoundland, Canada (47.697222 °N, -
500 52.921944 °W) via diving. Sampling of *Anarhichas minor* was performed in July, 2022, on a
501 captive-reared individual bred from broodstock collected in St-Lawrence Gulf, Banc Beaugé,
502 Canada (49.750000 °N, -60.166667 °W). Tissue was ground using dry ice. Cells were gently added
503 to pre-warmed 0.8% agarose and mixture was placed into the wells of a pre-chilled plug mold.
504 Following solidification, plugs were dislodged and treated with proteinase K and EDTA at 50°C.
505 HMW DNA was extracted by dissolving the plugs at 70°C to remove the agarose followed by a
506 phenol-chloroform extraction. Purification was performed on 15.0 µg of gDNA with AMPure PB
507 beads and a bead-to-template ratio of 1. The DNA libraries were prepared following the Pacific

508 Biosciences Preparing HiFi SMRTbell® Libraries using the SMRTbell Express Template Prep Kit
509 2.0 protocol. 10.0 µg of high molecular weight purified genomic DNA (final volume of 120 µl)
510 was sheared using the Diagenode Megaruptor 3 instrument (Diagenode Inc., Denville, NJ, USA)
511 and a two-cycle shear method at speed 33 followed by speed 34. The DNA Damage repair, End
512 repair and SMRT bell ligation steps were performed as described in the template preparation
513 protocol with the SMRTbell Template Prep Kit 2.0 reagents (Pacific Biosciences, Menlo
514 Park, CA, USA). The DNA libraries were size selected on a BluePippin system using a 10 kb
515 cutoff. The libraries underwent an AMPure PB bead cleanup following the SMRTlink v10
516 calculator procedure before being sequenced on a PacBio Sequel II instrument using adaptive
517 loading, Sequel II Sequencing Kit 2.0, SMRT Cell 8M and 30 hours movies with a pre-extension
518 time of 2h. Sequence data was processed using the SMRT Link Analysis
519 v. 10.1.0.119588 pipeline.

520 *Bathymaster signatus* was collected in Alaska, USA (52.1861 °N, -173.596 °W), by the
521 Alaska Trawl Survey on July 28th, 2012, via trawl net. DNA was extracted from gill filament via
522 the Circulomics Nanobind Tissue Kit. HiFi Library prep was done with SMRTbell prep kit 3.0
523 (version 102-166-600 Apr 2022). As part of the library prep, the genomic DNA was sheared to
524 25kb on a Megaruptor 2.0. The library was size selected on the Blue Pippin according to PacBio's
525 recommended settings (10kb-50kb collection). The sample was sequenced on one SMRT cell on
526 the Sequel II with v5 primer, v2.2 polymerase, 1 hr binding time, a 30 hr movie, 2 hr pre-extension,
527 and adaptive loading.

528 *Lycodes diapterus* was collected in Monterey Bay, California, USA (36.8009 °N, -
529 121.903867 °W), on October, 20th, 2021. High molecular weight DNA was extracted from
530 dissected muscle tissue using a Qiagen Genomic-tip DNA extraction kit. DNA was then sheared

531 to ~20 kbp using a Diagenode Megaruptor 3 and size selected for DNA for fragments greater than
532 10 kb using a BluePippin system. A PacBio HiFi library was prepared with the SMRTbell Express
533 Template Prep Kit 2.0. The library was then sequenced on a PacBio Sequel II instrument on an
534 8M SMRT cell in CCS mode with a 30-hour movie time. DNA extraction, library preparation, and
535 long-read sequencing of *Ophthalmolycus amberensis* are described in detail by Hotaling et al.
536 (2023).

537 Haplotype-phased genomes of all species except for *O. amberensis* were assembled from
538 long-read libraries using hifiasm v0.19.5-r592 (Cheng et al. 2021) set to default parameters.
539 Assemblies of primary contigs are reported here. Read processing and genome assembly of *O.*
540 *amberensis* was achieved using Canu (Koren et al. 2017) v1.8 and is described in detail in
541 Hotaling, et al. (2023). Assembly completeness was evaluated using BUSCO v5.4.7 (Simão et al.
542 2015) input with universal, single-copy Actinopterygii orthologs. Collection coordinates for the
543 specimens sequenced and reported in this study, and the *O. amberensis* specimen reported by
544 Hotaling et al. (2023), are visualized in Figure S11.

545 *4.2. AFP III and sasa/b annotation* - Homologs of AFP III were annotated in each genome
546 assembly included in the study using Exonerate v2.78.4 input with a query sequence of the
547 translated *Macrozoarces americanus* AFP III (J03924.1) set to the model parameter
548 'protein2genome' (Slater and Birney 2005). *sasa*, *sasb*, and genes flanking the 5' and 3' ends of
549 the ancestral syntenic region of Zoarcoidei AFP III (*sncgb* and *ldb3b*) were annotated using
550 Exonerate (Slater and Birney 2005) set to the same parameters input with protein sequences of *sas*
551 paralogs from *Lycodichthys dearborni* and *Gasterosteus aculeatus* protein sequences of *sncgb*
552 (XP_040031911.1) and *ldb3b* (XP_040031907.1) as shown in Figure 3A. Exonerate BED file
553 annotations of AFP III were filtered for whether hits contained start and stop codons and complete

554 sequences of exons 1 and 2. Translocated AFP III copies outside of the ancestral syntenic AFP III
555 region were manually reviewed for evidence of misassembly by aligning translocated AFP III
556 regions to (i) known, characterized AFP translocation in *A. lupus* (Desjardins et al. 2012) and (ii)
557 additional regions of translocation within single species if they possessed multiple translocation
558 events to identify artificial duplications. This ancestral region is defined as the locus of conserved
559 synteny at which AFP tandem arrays are flanked by the genes *sncgb* and *lbd3b*. Evidence of
560 artificial AFP III translocations driven by misassembly was not apparent. Pseudogenized copies
561 of AFP III were identified as regions mapping to AFP III query sequences that were complete but
562 lacked a start codon, lacked one of the two AFP III exons, exhibited truncations of the majority of
563 an exon, or conserved 5'/3' untranslated regions that lacked a proximal AFP coding sequence.
564 Publicly-available long-read genomes used in this study included *Cebidichthys violaceus*
565 (GCA_023349555.1), *Gasterosteus aculeatus* (GCA_016920845.1), *Leptoclinus maculatus*
566 (GCA_032191485.1), *Lycodes pacificus* (GCA_028022725.1), *Melanostigma gelatinosum*
567 (GCA_949748355.1), *Pholis gunnellus* (GCA_910591455.2).

568 *4.3. Environmental data* - Depth-informed temperatures and salinities were mined from the
569 Copernicus Global Ocean Reanalysis (GLORYS) database (Jean-Michel et al. 2021) within ±1°
570 latitude/longitude of species' coordinate of maximum likelihood of occurrence and the expected
571 depth range of each species spanning a 10 year period between June 1st 2011 - June 1st 2021.
572 Coordinates of maximum likelihood of occurrence were extracted from AquaMaps standardized
573 range predictions (Kaschner et al. 2013), which are probabilistic predictions of abundance and
574 occurrence derived from Global Biodiversity Information Facility occurrence data (Anon).
575 AquaMaps ranges were constrained within coordinates of known species occurrences. Species
576 minimum and maximum habitat depths were extracted from the FishBase (Froese 1996) depth

range variable (Froese 1996). For *Lycenchelys platyrhina*, which lacked sufficient FishBase data, minimum and maximum observed depths were extracted from GBIF (Anon). Thermal minima were calculated as the minimum temperature experienced by each species within their representative latitude-longitude-depth range. Pressure was calculated as a function of sea water depth and latitude using conversions defined by the UNESCO Joint Panel on Oceanographic Tables and Standards (Fofonoff 1983) and expressed as a mean.

4.4. Species tree construction and phylogenetic modeling - A maximum likelihood species tree was constructed from MUSCLE v5 (Edgar 2004) alignments of concatenated protein sequences of 3,603 universal Actinopterygii single copy orthologs using IQ-Tree2 v1.6.12 parameterized with a WAG substitution model and fixed rate heterogeneity (Nguyen et al. 2015; Minh et al. 2020). A Bayesian phylogenetically-corrected model was then fitted to predict AFP III copy number variation as a function of species' habitat temperature and pressure. The model assumed negative binomial variance for the AFP III count data and uninformative, uniform priors. Phylogenetic relatedness was fitted as a random effect of the genetic distance matrix derived from the species tree. The thermal minima and mean pressure of species' habitats were included as fixed effects, with pressure fitted as a second order polynomial function. An iteration of this model was fitted that predicted AFP III copy number as a function of both pressure and depth. Because pressure and depth correlate, this model iteration was fitted to evaluate whether controlling for depth removed or reduced the effect of pressure. Pressure exhibited a significant and equivalent effect after controlling for depth, demonstrating that it is a stronger predictor of AFP copy number than depth. Model selection performed using Bayesian marginal likelihoods (Berger and Pericchi 1996) revealed that pressure was a better predictor of AFP III copy number than depth.

599 A multivariate iteration of the phylogenetic model was also fitted to predict two separate
600 outcome variables for copy numbers of (i) AFP III within its ancestral, syntenic region and (ii)
601 AFP III genes translocated out of the syntenic region. This multivariate model did not permit
602 residual correlations. A third iteration of the phylogenetic model fit structural equations predicting
603 variation in AFP III copy number as a function of phylogenetically independent variation in habitat
604 thermal minimum and pressure. Phylogenetically independent variance in abiotic environments
605 were estimated by predicting environmental variables as a function of phylogeny, and AFP III
606 copy number as a function of environment and phylogeny. Thus, any effect of thermal minimum
607 or pressure on AFP III copy number is quantified after conditioning on phylogenetic variation in
608 abiotic environment.

609 Posterior sampling across all models was performed using four MCMC chains and 40,000
610 iterations including 10,000 warmups. All models were fitted using brms v2.20.4 (Bürkner 2017),
611 an R interpreter of the Stan Bayesian programming language (Carpenter et al. 2017). The
612 significance of fixed effects was assessed using a probability of direction test such that effects
613 described as 'significant' exhibited posterior probabilities with 95% confidence intervals above or
614 below 0 (Makowski, M.S. Ben-Shachar, et al. 2019). Because of potential misidentification of *L.*
615 *platyrhina*, we evaluated the effect of the identification on model predictions. The leverage (the
616 effect of a single observation on model predictions) that *L. platyrhina* imposed on parameter
617 estimation in phylogenetic models of AFP gene family evolution across environments was
618 quantified using a leave-one-out analysis. Removal of *L. platyrhina* from the univariate model
619 imposed a 6.45% reduction in the effect of thermal minima on AFP III copy number and 4.24%
620 reduction in the linear effect of pressure.

621 *4.5. Analyses of AFP III gene family evolution and synteny* - FASTA sequences of AFP III
622 exons 1 and 2 and *sasa*/*b* exons 1 and 6 were extracted from annotation bed files using bed2fasta
623 from bedtools v2.31.1 (Quinlan and Hall 2010). The two exons were concatenated per gene and
624 input to a codon-aware alignment using PRANK v.170427 (Löytynoja 2014; Löytynoja 2021). A
625 consensus gene tree was constructed from the alignment using IQ-TREE2 v1.6.12 set to fixed rate
626 heterogeneity, 1000 bootstraps and optimization of a codon-to-protein substitution model, which
627 selected a JTTDCMut+G4 model (Nguyen et al. 2015; Minh et al. 2020). Restricted maximum
628 likelihood ancestral state reconstructions of AFP III copy number, habitat thermal minimum, and
629 mean habitat pressure were performed using the 'ace' function of the R package ape v5.7-1
630 (Paradis et al. 2004; Paradis and Schliep 2019) in order to model contractions and expansions of
631 AFP III across the studied phylogeny. A density tree visualizing all 1000 bootstrap gene trees and
632 the consensus tree is plotted in Fig. S12. Ancestral state reconstructions of AFP III positions at the
633 ancestral Zoarcoidei node were performed using ace(). Individual, discrete reconstructions were
634 performed on 7 binary characters associated with whether species possessed putatively functional
635 copies of AFP III at the syntenically-conserved locus or the six translocation loci. The relative
636 likelihoods of the Zoarcoidei common ancestor possessing AFP III at these regions was measured
637 as a ratio of maximum likelihoods for AFP III presence at the syntenically-conserved region
638 divided by maximum likelihood of presence at each of the six translocation loci.
639 A multiple alignment of scaffolds or contigs containing translocated AFP III copies was
640 performed using progressiveMAUVE v2.4.0 (Darling et al. 2010), which identified conservation
641 and synteny of genomic regions conserved in at least two species of Zoarcoidei that exhibited
642 translocated AFPs. This multiple alignment and the positions of translocated AFP arrays relative

643 to conserved, syntenic regions are plotted in Fig. 3B in order to visualize conserved synteny of the
644 ancestral AFP III locus, as well as the locations and number of AFP III translocations.

645 *4.6. Models of selection on AFP III copy number and sequence* - Stabilizing selection on
646 AFP III copy number was modeled using Bayesian Ornstein-Uhlenbeck phylogenetic mixed
647 models implemented in POUMM v.2.1.7 set to MCMC equals TRUE, 4 MCMC chains, and
648 80,000 samples (Mitov and Stadler 2018; Mitov and Stadler 2019). Significant differences
649 between posterior probabilities of stabilizing selection on translocated and syntenic copy number
650 were evaluated using a Bayes factor test implemented in bayestestR v0.13.2 (Makowski, M. Ben-
651 Shachar, et al. 2019).

652 Purifying and diversifying selection were modeled across the AFP III gene tree by
653 estimating branch-tip specific d_N/d_S ratios in hyphy v2.5.62 RELAX (K. et al. 2005; Wertheim et
654 al. 2015; Kosakovsky Pond et al. 2020). In this paper, we report branch-tip d_N/d_S ratios as measures
655 of purifying vs. diversifying selection, but we did not use RELAX to perform a statistical test of
656 relaxed selection among a group of genes. As input to RELAX, we used a codon-aware alignment
657 of all *sasa*, *sasb*, and AFP homologs produced using PRANK v.170427 (Löytynoja 2014;
658 Löytynoja 2021) input with parameters -F and -codon and a guide tree produced using an IQ-Tree2
659 phylogenetic model fit to the PRANK alignment, parameterized with nucleotide substitution
660 model optimization which selected a K2P+G4 model, fixed rate heterogeneity, and 1000
661 bootstraps (Edgar 2004; Löytynoja 2014; Löytynoja 2021). A nucleotide substitution model was
662 selected because it produced more conservative d_N/d_S estimates (i.e., less extreme absolute
663 estimates of selection)(Katoh et al. 2002), which was used to produce the Figure 3C gene tree.
664 Syntenic and translocated AFP homologs were defined as test and reference features with *sas*
665 genes incorporated as background. Reported d_N/d_S ratios were output by the RELAX general

666 descriptive model (Wertheim et al. 2015). Variation in AFP d_N/d_S was modeled as a function of
667 whether copies fell within syntenic or translocated loci and gene branch tip lengths using gamma
668 distributed Bayesian model specified as described under 'Species tree construction and
669 phylogenetic modeling'.
670

671 **Acknowledgements**

672 We acknowledge funding from National Science Foundation awards OPP-1543383 and
673 OPP-1947040 (supporting TD), and OPP-2312253 (to JLK) as well as funding from the Antarctic
674 Science Bursary. We acknowledge computing resources from the Center for Institutional Research
675 Computing at Washington State University, the National Science Foundation Extreme Science and
676 Engineering Discovery Environment (XSEDE), and University of California, Santa Cruz Research
677 Computing. We thank the veterinary clinic staff of the Biodôme de Montréal, including Karine
678 Béland, DMV. We also thank the captain and crew of the ARSV *Laurence M. Gould*, the personnel
679 of the U.S. Antarctic Program Support Contractors for assistance in Chile, at sea and at Palmer
680 Station, as well as the logistics in Denver, CO, for their support related to the Antarctic fieldwork
681 required for this study. We acknowledge funding from the Trond Mohn Science Foundation
682 through the Centre for Deep Sea Research (grant number TMS2020TMT13) and the Norwegian
683 Biodiversity Information Centre (the Taxonomy Initiative, project nr. 3-20-70184243) and thank
684 the scientists and students from University of Bergen (Norway), the crew of the RV GO Sars and
685 the pilots of the ROV ÆGIR6000 for their assistance with sampling in the Arctic. Lastly, we would
686 like to thank the Alaskan Trawl Survey, and the Ocean Genome Legacy Center, Northeastern
687 University, for assisting with specimen collections and archiving.
688

689 **Author Contributions**

690 Designed research (JLK, SNB)

691 Performed research (FGH, LSFL, IB, JLK, MHE, NRLF, NS, PBF, SH, SNB, TA, TD)

692 Analyzed data (JLK, NS, SNB)

693 Wrote the paper (JLK, NS, SNB)

694 Edited the paper (FGH, LSFL, IB, JLK, MHE, NRLF, NS, PBF, SH, SNB, TA, TD)

695

696 **Data Availability**

697 Genome assemblies, raw sequencing reads, and associated files are available on NCBI under the
698 following Bioprojects: PRJNA980960 (*Anarhichas lupus*), PRJNA982125 (*Anarhichas minor*),
699 PRJNA982427 (*Bathymaster signatus*), PRJNA985917 (*Lycenchelys platyrhina*), PRJNA982746
700 (*Lycodes diapterus*) and PRJNA701078 (*Ophalmolycus amberensis*). All code used for
701 bioinformatic processing and statistical analysis are available under the GitHub repository
702 https://github.com/snbogan/Long_AFP [available to reviewers upon request or acceptance and
703 publication] in addition to intermediate data files and specimen metadata. An archived copy of this
704 repository is available on Zenodo under the DOI [to be generated upon acceptance].

705

706

707

708

709

710

711

712

713 **References**

714 Altschul SF, Gish W, Miller W, Myers EW, Lipman DJ. 1990. Basic local alignment search tool.
715 *J. Mol. Biol.* 215:403–410.

716 Anderson ME. 1994. Systematics and osteology of the Zoarcidae (Teleostei: Perciformes). *JLB*
717 *Smith Institute of Ichthyology, Ichthyological Bulletin* 60:1–120.

718 Anon. GBIF.org. *Global Biodiversity Information Facility* [Internet]. Available from:
719 https://www.gbif.org

720 Auger M, Morrow R, Kestenare E, Sallée J-B, Cowley R. 2021. Southern Ocean in-situ
721 temperature trends over 25 years emerge from interannual variability. *Nat. Commun.*
722 12:514.

723 Baalsrud HT, Tørresen OK, Solbakken MH, Salzburger W, Hanel R, Jakobsen KS, Jentoft S.
724 2018. De Novo Gene Evolution of Antifreeze Glycoproteins in Codfishes Revealed by
725 Whole Genome Sequence Data. *Mol. Biol. Evol.* 35:593–606.

726 Barrett J. 2001. Thermal hysteresis proteins. *Int. J. Biochem. Cell Biol.* 33:105–117.

727 Baskaran A, Kaari M, Venugopal G, Manikkam R, Joseph J, Bhaskar PV. 2021. Anti freeze
728 proteins (Afp): Properties, sources and applications - A review. *Int. J. Biol. Macromol.*
729 189:292–305.

730 Berger JO, Pericchi LR. 1996. The Intrinsic Bayes Factor for Model Selection and Prediction. *J.*
731 *Am. Stat. Assoc.* 91:109–122.

732 Bista I, Collins M, Wellcome Sanger Institute Tree of Life Management, Samples and
733 Laboratory team. 2024. The genome sequence of the limp eelpout, Melanostigma
734 gelatinosum Günther, 1881. *Wellcome Open Research* 9:192.

735 Bista I, Wood JMD, Desvignes T, McCarthy SA, Matschiner M, Ning Z, Tracey A, Torrance J,
736 Sims Y, Chow W, et al. 2023. Genomics of cold adaptations in the Antarctic notothenioid
737 fish radiation. *Nat. Commun.* 14:3412.

738 Bodnar RJ. 1993. Revised equation and table for determining the freezing point depression of
739 H2O-Nacl solutions. *Geochim. Cosmochim. Acta* 57:683–684.

740 Bürkner P-C. 2017. brms: An R Package for Bayesian Multilevel Models Using Stan. *J. Stat.*
741 *Softw.* 80:1–28.

742 Carpenter B, Gelman A, Hoffman MD, Lee D, Goodrich B, Betancourt M, Brubaker MA, Guo J,
743 Li P, Riddell A. 2017. Stan: A Probabilistic Programming Language. *J. Stat. Softw.*
744 [Internet] 76. Available from: http://dx.doi.org/10.18637/jss.v076.i01

745 Celik Y, Graham LA, Mok Y-F, Bar M, Davies PL, Braslavsky I. 2010. Superheating of ice
746 crystals in antifreeze protein solutions. *Proc. Natl. Acad. Sci. U. S. A.* 107:5423–5428.

Cheng C, Devries A. 2002. Origins and evolution of fish antifreeze proteins. *Fish antifreeze proteins*:83–107.

Cheng H, Concepcion GT, Feng X, Zhang H, Li H. 2021. Haplotype-resolved de novo assembly using phased assembly graphs with hifiasm. *Nat. Methods* 18:170–175.

Cziko PA, DeVries AL, Evans CW, Cheng C-HC. 2014. Antifreeze protein-induced superheating of ice inside Antarctic notothenioid fishes inhibits melting during summer warming. *Proc. Natl. Acad. Sci. U. S. A.* 111:14583–14588.

Darling AE, Mau B, Perna NT. 2010. progressiveMauve: multiple genome alignment with gene gain, loss and rearrangement. *PLoS One* 5:e11147.

Davies PL. 2022. Reflections on antifreeze proteins and their evolution. *Biochem. Cell Biol.* 100:282–291.

Deng C, Cheng C-HC, Ye H, He X, Chen L. 2010. Evolution of an antifreeze protein by neofunctionalization under escape from adaptive conflict. *Proc. Natl. Acad. Sci. U. S. A.* 107:21593–21598.

Desjardins M, Graham LA, Davies PL, Fletcher GL. 2012. Antifreeze protein gene amplification facilitated niche exploitation and speciation in wolffish. *FEBS J.* 279:2215–2230.

DeVries AL. 1971. Glycoproteins as biological antifreeze agents in antarctic fishes. *Science* 172:1152–1155.

DeVries AL, Cheng C -H C. 2005. Antifreeze Proteins and Organismal Freezing Avoidance in Polar Fishes. In: Fish Physiology. Vol. 22. Academic Press. p. 155–201.

DeVries AL, Wohlschlag DE. 1969. Freezing resistance in some Antarctic fishes. *Science* 163:1073–1075.

Duman JG. 2015. Animal ice-binding (antifreeze) proteins and glycolipids: an overview with emphasis on physiological function. *J. Exp. Biol.* 218:1846–1855.

Edgar RC. 2004. MUSCLE: multiple sequence alignment with high accuracy and high throughput. *Nucleic Acids Res.* 32:1792–1797.

Fetterer F;. KK;. MW;. SM;. WA. 2017. Sea Ice Index, Version 3. Available from: https://nsidc.org/data/g02135/versions/3

Fofonoff NP. 1983. Algorithms for the computation of fundamental properties of seawater. Available from: https://repository.oceanbestpractices.org/handle/11329/109

Friedman ST, Muñoz MM. 2023. A latitudinal gradient of deep-sea invasions for marine fishes. *Nat. Commun.* 14:773.

Froese R. 1996. FishBase. *Oceanographic Literature Review* 3:321.

780 Fujino K, Lewis EL, Perkin RG. 1974. The freezing point of seawater at pressures up to 100
781 bars. *J. Geophys. Res.* 79:1792–1797.

782 Gilbert JA, Davies PL, Laybourn-Parry J. 2005. A hyperactive, Ca2+-dependent antifreeze
783 protein in an Antarctic bacterium. *FEMS Microbiol. Lett.* 245:67–72.

784 Gillett MB, Suko JR, Santoso FO, Yancey PH. 1997. Elevated levels of trimethylamine oxide in
785 muscles of deep-sea gadiform teleosts: A high-pressure adaptation? *J. Exp. Zool.* 279:386–
786 391.

787 Graham LA, Davies PL. 2024. Fish antifreeze protein origin in sculpins by frameshifting within
788 a duplicated housekeeping gene. *FEBS J.* 291:4043–4061.

789 Griffith RW. 1981. Composition of the blood serum of deep-sea fishes. *Biol. Bull.* 160:250–264.

790 Gupta R, Deswal R. 2014. Antifreeze proteins enable plants to survive in freezing conditions. *J.*
791 *Biosci.* 39:931–944.

792 Harewood L, Schütz F, Boyle S, Perry P, Delorenzi M, Bickmore WA, Reymond A. 2010. The
793 effect of translocation-induced nuclear reorganization on gene expression. *Genome Res.*
794 20:554–564.

795 Hargens AR. 1972. Freezing resistance in polar fishes. *Science* 176:184–186.

796 Hastings PJ, Ira G, Lupski JR. 2009. A microhomology-mediated break-induced replication
797 model for the origin of human copy number variation. *PLoS Genet.* 5:e1000327.

798 Hastings PJ, Lupski JR, Rosenberg SM, Ira G. 2009. Mechanisms of change in gene copy
799 number. *Nat. Rev. Genet.* 10:551–564.

800 Hayes PH, Davies PL, Fletcher GL. 1991. Population differences in antifreeze protein gene copy
801 number and arrangement in winter flounder. *Genome* 34:174–177.

802 Hew CL, Wang NC, Joshi S, Fletcher GL, Scott GK, Hayes PH, Buettner B, Davies PL. 1988.
803 Multiple genes provide the basis for antifreeze protein diversity and dosage in the ocean
804 pout, Macrozoarces americanus. *J. Biol. Chem.* 263:12049–12055.

805 Hickerson MJ, Cunningham CW. 2006. Nearshore fish (*Pholis gunnellus*) persists across the
806 North Atlantic through multiple glacial episodes: N. ATLANTIC PERSISTENCE
807 INPHOLIS GUNNELLUS. *Mol. Ecol.* 15:4095–4107.

808 Hobbs RS, Hall JR, Graham LA, Davies PL, Fletcher GL. 2020. Antifreeze protein dispersion in
809 eelpouts and related fishes reveals migration and climate alteration within the last 20 Ma.
810 *PLoS One* 15:e0243273.

811 Hotaling S, Borowiec ML, Lins LSF, Desvignes T, Kelley JL. 2021. The biogeographic history
812 of eelpouts and related fishes: Linking phylogeny, environmental change, and patterns of
813 dispersal in a globally distributed fish group. *Mol. Phylogenet. Evol.* 162:107211.

814 Hotaling S, Desvignes T, Sproul JS, Lins LSF, Kelley JL. 2023. Pathways to polar adaptation in
815 fishes revealed by long-read sequencing. *Molecular Ecology* 32:1381–1397.

816 Hull RM, Cruz C, Jack CV, Houseley J. 2017. Environmental change drives accelerated
817 adaptation through stimulated copy number variation. *PLoS Biol.* 15:e2001333.

818 Jean-Michel L, Eric G, Romain B-B, Gilles G, Angélique M, Marie D, Clément B, Mathieu H,
819 Olivier LG, Charly R, et al. 2021. The Copernicus Global 1/12° Oceanic and Sea Ice
820 GLORYS12 Reanalysis. *Front Earth Sci. Chin.* [Internet] 9. Available from:
821 https://www.frontiersin.org/articles/10.3389/feart.2021.698876

822 Jia Z, DeLuca CI, Chao H, Davies PL. 1996. Structural basis for the binding of a globular
823 antifreeze protein to ice. *Nature* 384:285–288.

824 Kaschner K, Rius-Barile J, Kesner-Reyes K. 2013. About AquaMaps. Available from:
825 https://www.aquamaps.org/AboutAquaMaps.htm

826 Katoh K, Misawa K, Kuma K-I, Miyata T. 2002. MAFFT: a novel method for rapid multiple
827 sequence alignment based on fast Fourier transform. *Nucleic Acids Res.* 30:3059–3066.

828 Kelley JL, Aagaard JE, MacCoss MJ, Swanson WJ. 2010. Functional diversification and
829 evolution of antifreeze proteins in the antarctic fish Lycodichthys dearborni. *J. Mol. Evol.*
830 71:111–118.

831 Kidwell MG. 2002. Transposable elements and the evolution of genome size in eukaryotes.
832 *Genetica* 115:49–63.

833 Kondrashov FA. 2012. Gene duplication as a mechanism of genomic adaptation to a changing
834 environment. *Proc. Biol. Sci.* 279:5048–5057.

835 Koren S, Walenz BP, Berlin K, Miller JR, Bergman NH, Phillippy AM. 2017. Canu: scalable
836 and accurate long-read assembly via adaptive k-mer weighting and repeat separation.
837 *Genome Res.* 27:722–736.

838 Kosakovsky Pond SL, Poon AFY, Velazquez R, Weaver S, Hepler NL, Murrell B, Shank SD,
839 Magalis BR, Bouvier D, Nekrutenko A, et al. 2020. HyPhy 2.5-A customizable platform for
840 evolutionary hypothesis testing using PHYlogenies. *Mol. Biol. Evol.* 37:295–299.

841 K. PSL, Frost SD, Muse SV. 2005. HyPhy: hypothesis testing using phylogenies. *Bioinformatics*
842 21:676–679.

843 Kramara J, Osia B, Malkova A. 2018. Break-Induced Replication: The Where, The Why, and
844 The How. *Trends Genet.* 34:518–531.

845 Lauer S, Gresham D. 2019. An evolving view of copy number variants. *Curr. Genet.* 65:1287–
846 1295.

847 Löytynoja A. 2014. Phylogeny-aware alignment with PRANK. *Methods Mol. Biol.* 1079:155–

170.

Löytynoja A. 2021. Phylogeny-aware alignment with PRANK and PAGAN. *Methods Mol. Biol.* 2231:17–37.

Makowski D, Ben-Shachar M, Lüdecke D. 2019. BayestestR: Describing effects and their uncertainty, existence and significance within the Bayesian framework. *J. Open Source Softw.* 4:1541.

Makowski D, Ben-Shachar MS, Chen SHA, Lüdecke D. 2019. Indices of Effect Existence and Significance in the Bayesian Framework. *Front. Psychol.* 10:2767.

Marx V. 2023. Method of the year: long-read sequencing. *Nat. Methods* 20:6–11.

Mérot C, Oomen RA, Tigano A, Wellenreuther M. 2020. A roadmap for understanding the evolutionary significance of structural genomic variation. *Trends Ecol. Evol.* 35:561–572.

Minh BQ, Schmidt HA, Chernomor O, Schrempf D, Woodhams MD, von Haeseler A, Lanfear R. 2020. IQ-TREE 2: New Models and Efficient Methods for Phylogenetic Inference in the Genomic Era. *Mol. Biol. Evol.* 37:1530–1534.

Mitov V, Stadler T. 2018. A practical guide to estimating the heritability of pathogen traits. *Mol. Biol. Evol.* 35:756–772.

Mitov V, Stadler T. 2019. Parallel likelihood calculation for phylogenetic comparative models: The SPLITT C++ library. *Methods Ecol. Evol.* 10:493–506.

Møller PR, Nielsen JG, Anderson ME. 2005. Systematics of Polar Fishes. In: Fish Physiology. Vol. 22. Academic Press. p. 25–78.

Nath S, Shaw DE, White MA. 2021. Improved contiguity of the threespine stickleback genome using long-read sequencing. *G3 (Bethesda)* 11:jkab007.

Nguyen L-T, Schmidt HA, von Haeseler A, Minh BQ. 2015. IQ-TREE: a fast and effective stochastic algorithm for estimating maximum-likelihood phylogenies. *Mol. Biol. Evol.* 32:268–274.

Paradis E, Claude J, Strimmer K. 2004. APE: Analyses of Phylogenetics and Evolution in R language. *Bioinformatics* 20:289–290.

Paradis E, Schliep K. 2019. ape 5.0: an environment for modern phylogenetics and evolutionary analyses in R. *Bioinformatics* 35:526–528.

Ponte RM. 2013. Heat content and temperature of the ocean. In: Earth System Monitoring. New York, NY: Springer New York. p. 153–180.

Potter RW, Clynne MA, Brown DL. 1978. Freezing point depression of aqueous sodium chloride solutions. *Econ. Geol.* 73:284–285.

881 Programme WSIT of L, Potter S, Collective DT of LB, Collective WSISODP, Collective T of
882 LCI, of Life Consortium DT. 2022. The genome sequence of the rock gunnel, Pholis
883 gunnellus (Linnaeus, 1758). *Wellcome Open Res.* 7:58.

884 Quinlan AR, Hall IM. 2010. BEDTools: a flexible suite of utilities for comparing genomic
885 features. *Bioinformatics* 26:841–842.

886 Radchenko OA. 2016. Timeline of the evolution of eelpouts from the suborder Zoarcoidei
887 (Perciformes) based on DNA variability. *Journal of Ichthyology* 56:556–568.

888 Raymond JA, DeVries AL. 1977. Adsorption inhibition as a mechanism of freezing resistance in
889 polar fishes. *Proc. Natl. Acad. Sci. U. S. A.* 74:2589–2593.

890 Reist JD, Wrona FJ, Prowse TD, Power M, Dempson JB, Beamish RJ, King JR, Carmichael TJ,
891 Sawatzky CD. 2006. General effects of climate change on Arctic fishes and fish
892 populations. *Ambio* 35:370–380.

893 Rhie A, McCarthy SA, Fedrigo O, Damas J, Formenti G, Koren S, Uliano-Silva M, Chow W,
894 Fungtammasan A, Kim J, et al. 2021. Towards complete and error-free genome assemblies
895 of all vertebrate species. *Nature* 592:737–746.

896 Rivera-Colón AG, Rayamajhi N, Minhas BF, Madrigal G, Bilyk KT, Yoon V, Hüne M, Gregory
897 S, Cheng CHC, Catchen JM. 2023. Genomics of secondarily temperate adaptation in the
898 only non-Antarctic icefish. *Mol. Biol. Evol.* 40:msad029.

899 Rives N, Lamba V, Cheng CHC, Zhuang X. 2024. Diverse origins of near-identical antifreeze
900 proteins in unrelated fish lineages provide insights into evolutionary mechanisms of new
901 gene birth and protein sequence convergence. *Mol. Biol. Evol.* 41:msae182.

902 Schmidt JM, Good RT, Appleton B, Sherrard J, Raymant GC, Bogwitz MR, Martin J, Daborn
903 PJ, Goddard ME, Batterham P, et al. 2010. Copy number variation and transposable
904 elements feature in recent, ongoing adaptation at the Cyp6g1 locus. *PLoS Genet.*
905 6:e1000998.

906 Scholander PF, Flagg W, Hock RJ, Irving L. 1953. Studies on the physiology of frozen plants
907 and animals in the arctic. *J. Cell. Comp. Physiol.* 42:1–56.

908 Simão FA, Waterhouse RM, Ioannidis P, Kriventseva EV, Zdobnov EM. 2015. BUSCO:
909 assessing genome assembly and annotation completeness with single-copy orthologs.
910 *Bioinformatics* 31:3210–3212.

911 Slater GSC, Birney E. 2005. Automated generation of heuristics for biological sequence
912 comparison. *BMC Bioinformatics* 6:31.

913 Storey KB, Storey JM. 1988. Freeze tolerance in animals. *Physiol. Rev.* 68:27–84.

914 Verde C, Parisi E, di Prisco G. 2006. The evolution of thermal adaptation in polar fish. *Gene*
915 385:137–145.

916 Wang W, Chen L, Wang X, Duan J, Flynn RD, Wang Y, Clark CB, Sun L, Zhang D, Wang DR,
917 et al. 2021. A transposon-mediated reciprocal translocation promotes environmental
918 adaptation but compromises domesticability of wild soybeans. *New Phytol.* 232:1765–1777.

919 Wang Y, Wang X, Paterson AH. 2012. Genome and gene duplications and gene expression
920 divergence: a view from plants. *Ann. N. Y. Acad. Sci.* 1256:1–14.

921 Watson KB, Lehnert SJ, Bentzen P, Kess T, Einfeldt A, Duffy S, Perriman B, Lien S, Kent M,
922 Bradbury IR. 2022. Environmentally associated chromosomal structural variation influences
923 fine-scale population structure of Atlantic Salmon (Salmo salar). *Mol. Ecol.* 31:1057–1075.

924 Watson SK, deLeeuw RJ, Horsman DE, Squire JA, Lam WL. 2007. Cytogenetically balanced
925 translocations are associated with focal copy number alterations. *Hum. Genet.* 120:795–805.

926 Wertheim JO, Murrell B, Smith MD, Kosakovsky Pond SL, Scheffler K. 2015. RELAX:
927 detecting relaxed selection in a phylogenetic framework. *Mol. Biol. Evol.* 32:820–832.

928 Worster MG, Rees Jones DW. 2015. Sea-ice thermodynamics and brine drainage. *Philos. Trans.*
929 *A Math. Phys. Eng. Sci.* 373:20140166.

930 Wright DB, Escalona M, Marimuthu MPA, Sahasrabudhe R, Nguyen O, Sacco S, Beraut E,
931 Toffelmier E, Miller C, Shaffer HB, et al. 2023. Reference genome of the Monkeyface
932 Prickleback, Cebidichthys violaceus. *J. Hered.* 114:52–59.

933 Yancey PH, Blake WR, Conley J. 2002. Unusual organic osmolytes in deep-sea animals:
934 adaptations to hydrostatic pressure and other perturbants. *Comp. Biochem. Physiol. A Mol.*
935 *Integr. Physiol.* 133:667–676.

936 Yancey PH, Gerringer ME, Drazen JC, Rowden AA, Jamieson A. 2014. Marine fish may be
937 biochemically constrained from inhabiting the deepest ocean depths. *Proc. Natl. Acad. Sci.*
938 *U. S. A.* 111:4461–4465.

939 Zhuang X, Yang C, Murphy KR, Cheng C-HC. 2019. Molecular mechanism and history of non-
940 sense to sense evolution of antifreeze glycoprotein gene in northern gadids. *Proc. Natl.*
941 *Acad. Sci. U. S. A.* 116:4400–4405.

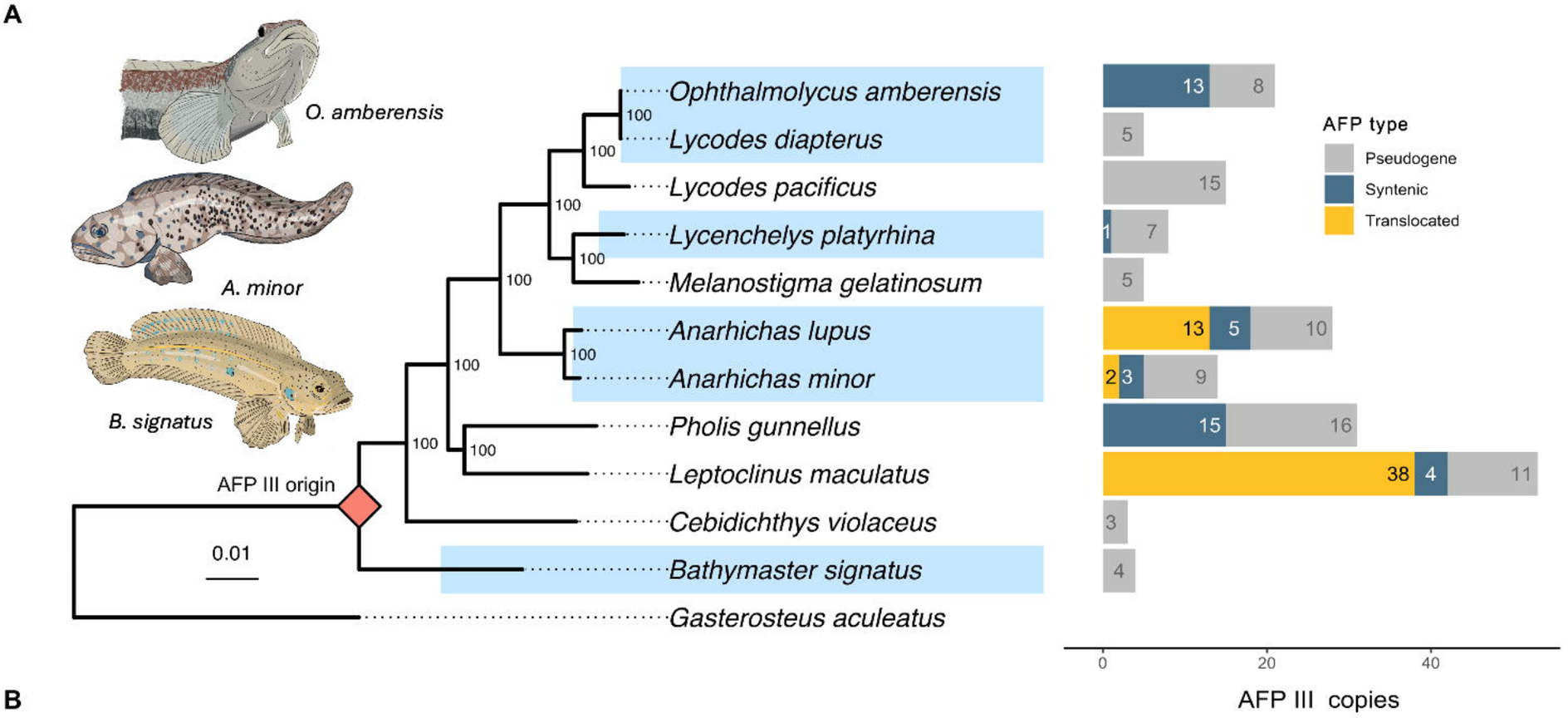
A
O. amberensis
A. minor
B. signatus
AFP III origin
0.01
Ophthalmolycus amberensis
Lycodes diapterus
Lycodes pacificus
Lycenchelys platyrhina
Melanostigma gelatinosum
Anarhichas lupus
Anarhichas minor
Pholis gunnellus
Leptoclinus maculatus
Cebidichthys violaceus
Bathymaster signatus
Gasterosteus aculeatus
100
AFP type
Pseudogene
Syntenic
Translocated
13 8
5
15
1 7
5
13 5 10
2 3 9
15 16
38 4 11
3
4
0
20
40
AFP III copies

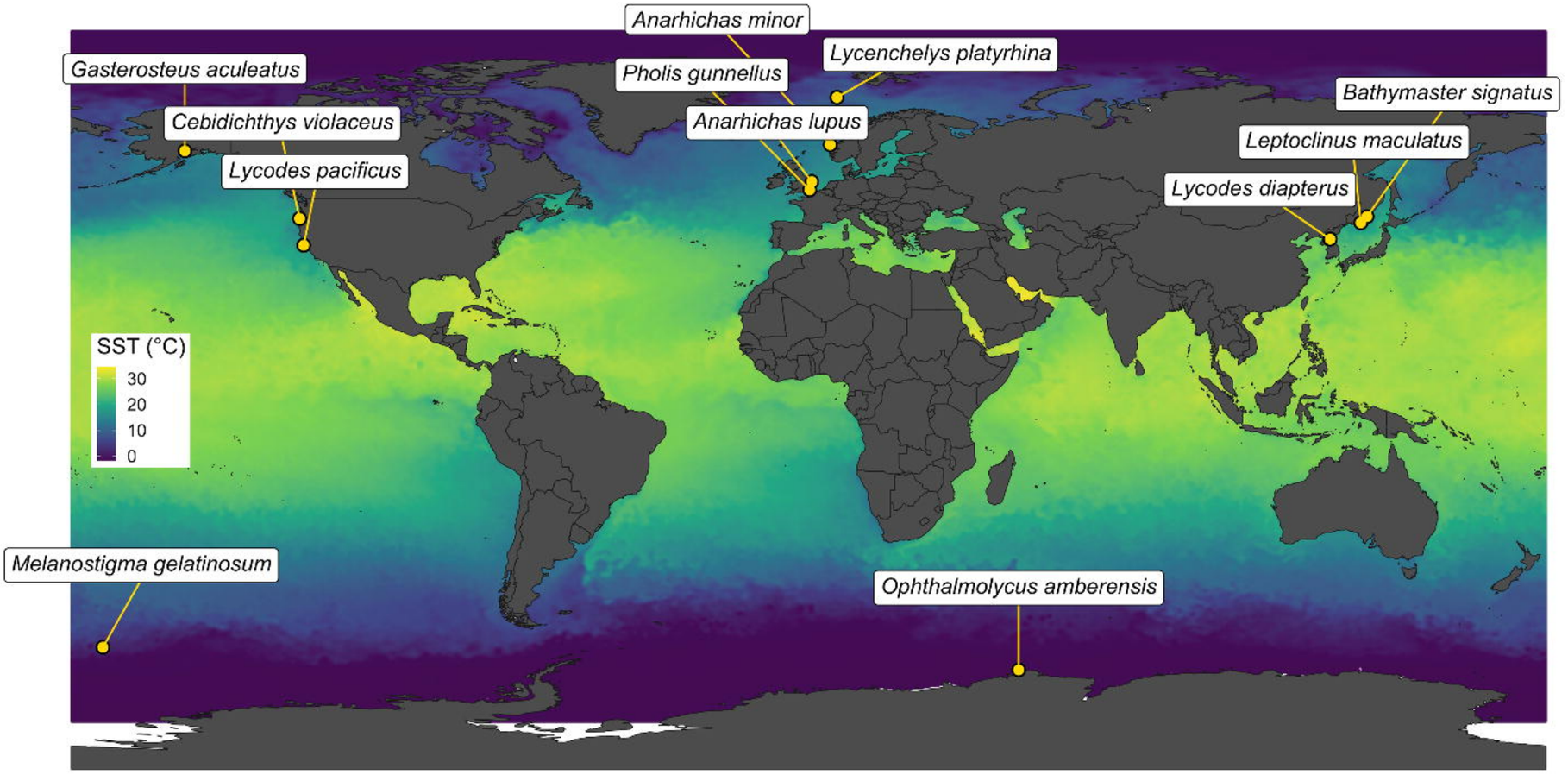
B
Anarhichas minor
Lycenchelys platyrhina
Gasterosteus aculeatus
Pholis gunnellus
Bathymaster signatus
Cebidichthys violaceus
Anarhichas lupus
Leptoclinus maculatus
Lycodes pacificus
Lycodes diapterus
SST (°C)
30
20
10
0
Melanostigma gelatinosum
Ophthalmolycus amberensis

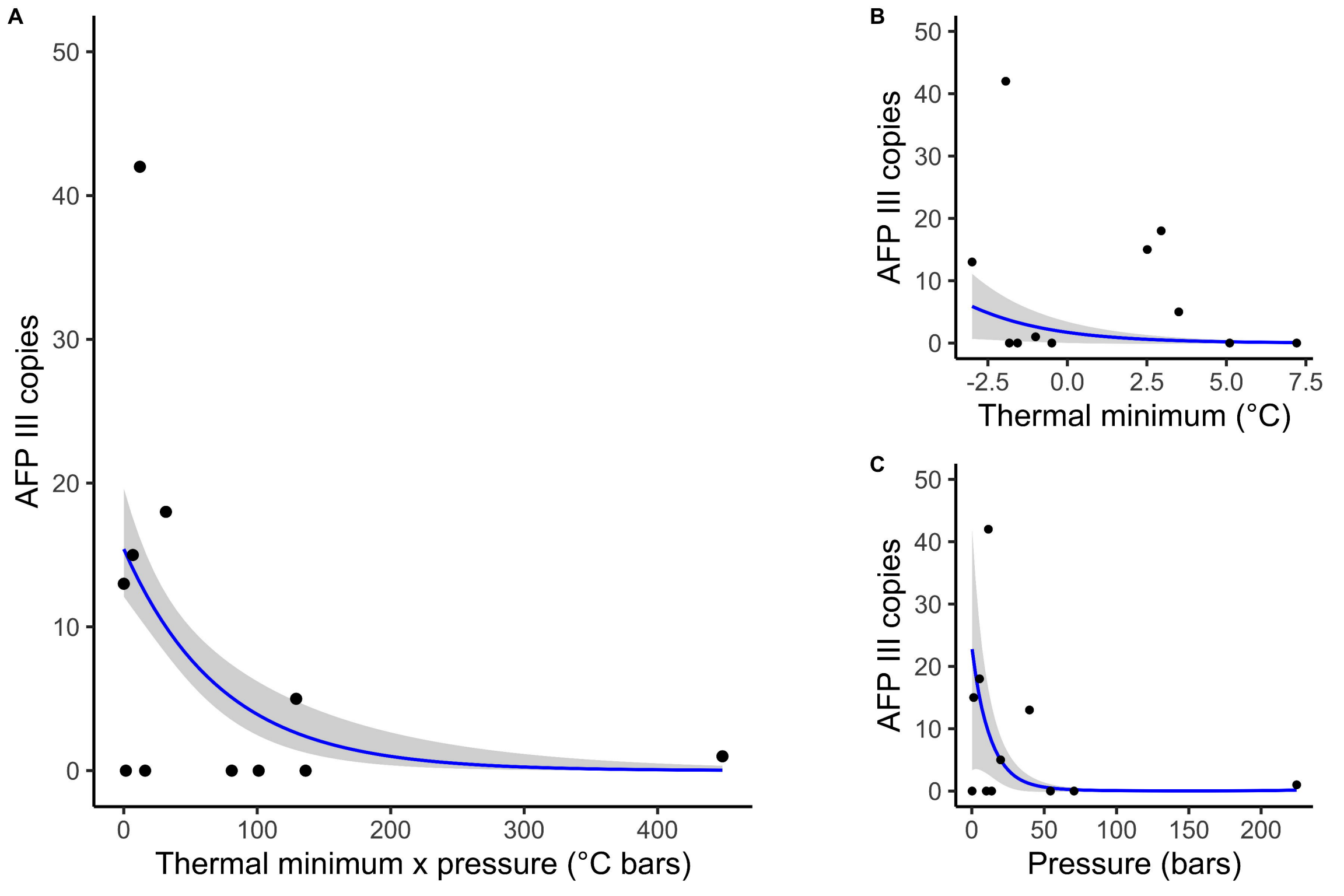
A
AFP III copies
50
40
30
20
10
0
0
100
200
300
400
Thermal minimum x pressure (°C bars)
B
AFP III copies
50
40
30
20
10
0
-2.5
0.0
2.5
5.0
7.5
Thermal minimum (°C)
C
AFP III copies
50
40
30
20
10
0
0
50
100
150
200
Pressure (bars)

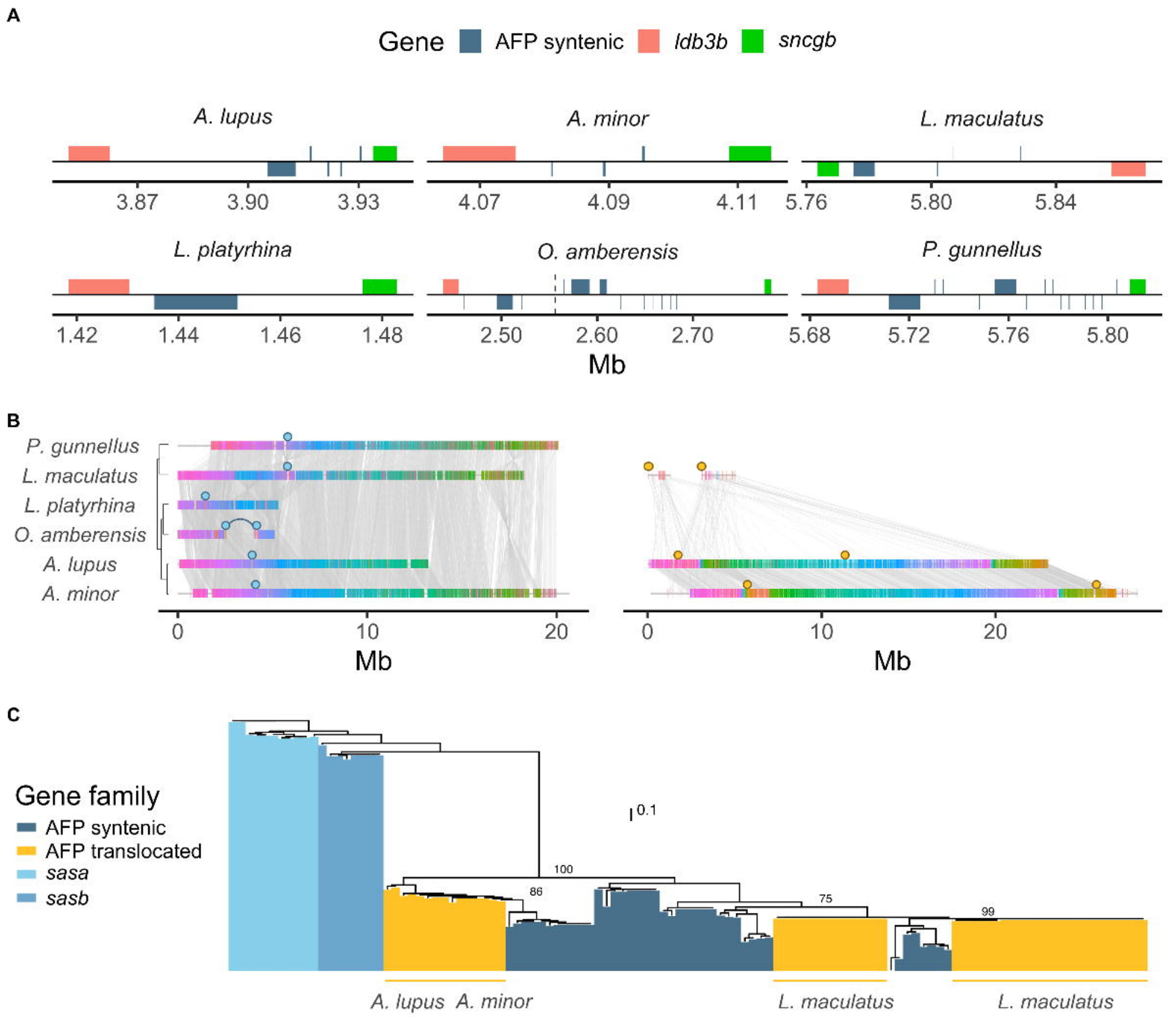
A
Gene
AFP syntenic
ldb3b
sncgb
A. lupus
3.87
3.90
3.93
A. minor
4.07
4.09
4.11
L. maculatus
5.76
5.80
5.84
L. platyrhina
1.42
1.44
1.46
1.48
O. amberensis
2.50
2.60
2.70
P. gunnellus
5.68
5.72
5.76
5.80
Mb
B
P. gunnellus
L. maculatus
L. platyrhina
O. amberensis
A. lupus
A. minor
0
10
20
Mb
0
10
20
Mb
C
Gene family
AFP syntenic
AFP translocated
sasa
sasb
0.1
100
86
75
99
A. lupus
A. minor
L. maculatus
L. maculatus

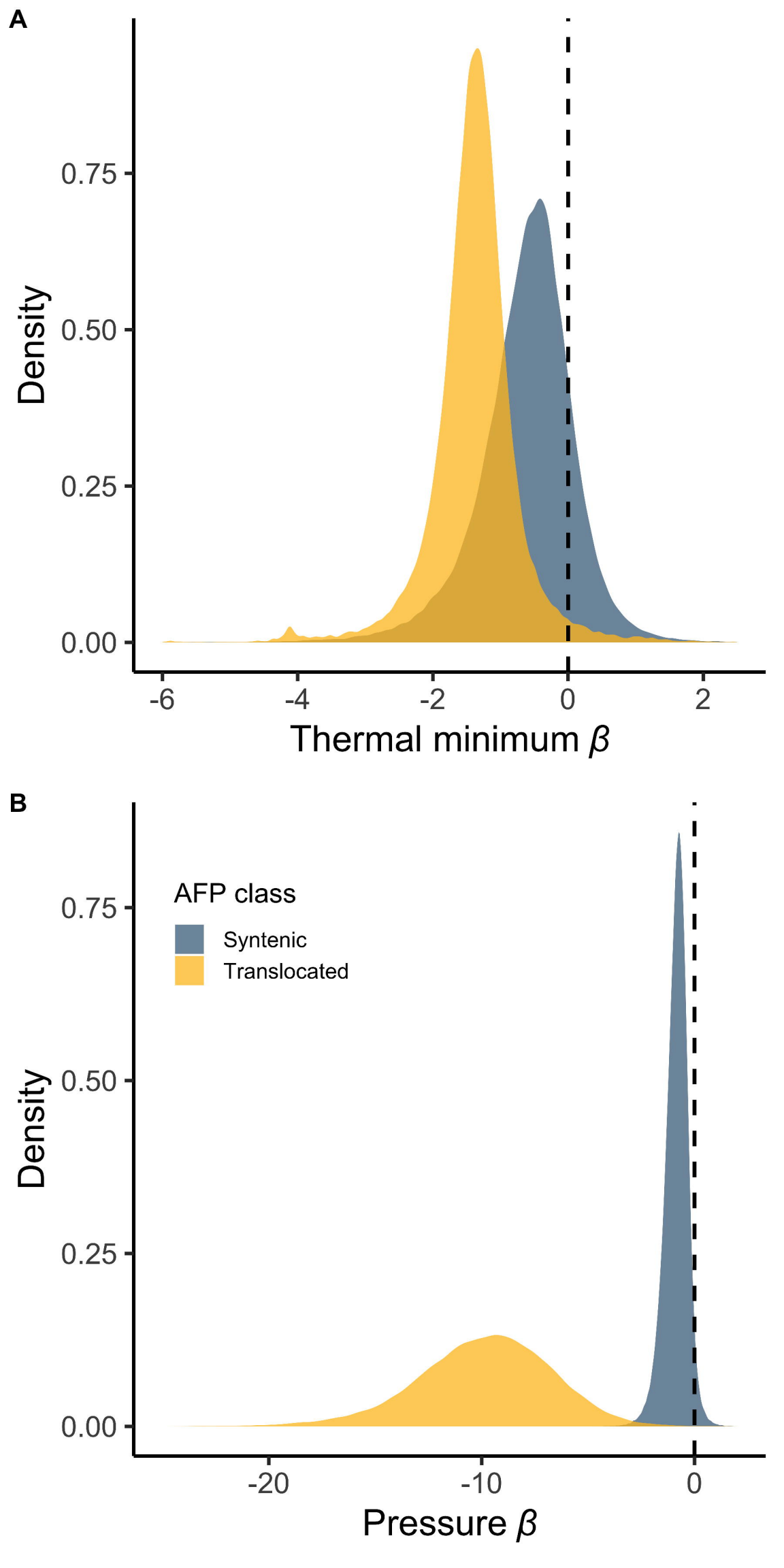
A
Density
0.75
0.50
0.25
0.00
-6
-4
-2
0
2
Thermal minimum β
B
AFP class
Syntenic
Translocated
Density
0.75
0.50
0.25
0.00
-20
-10
0
Pressure β

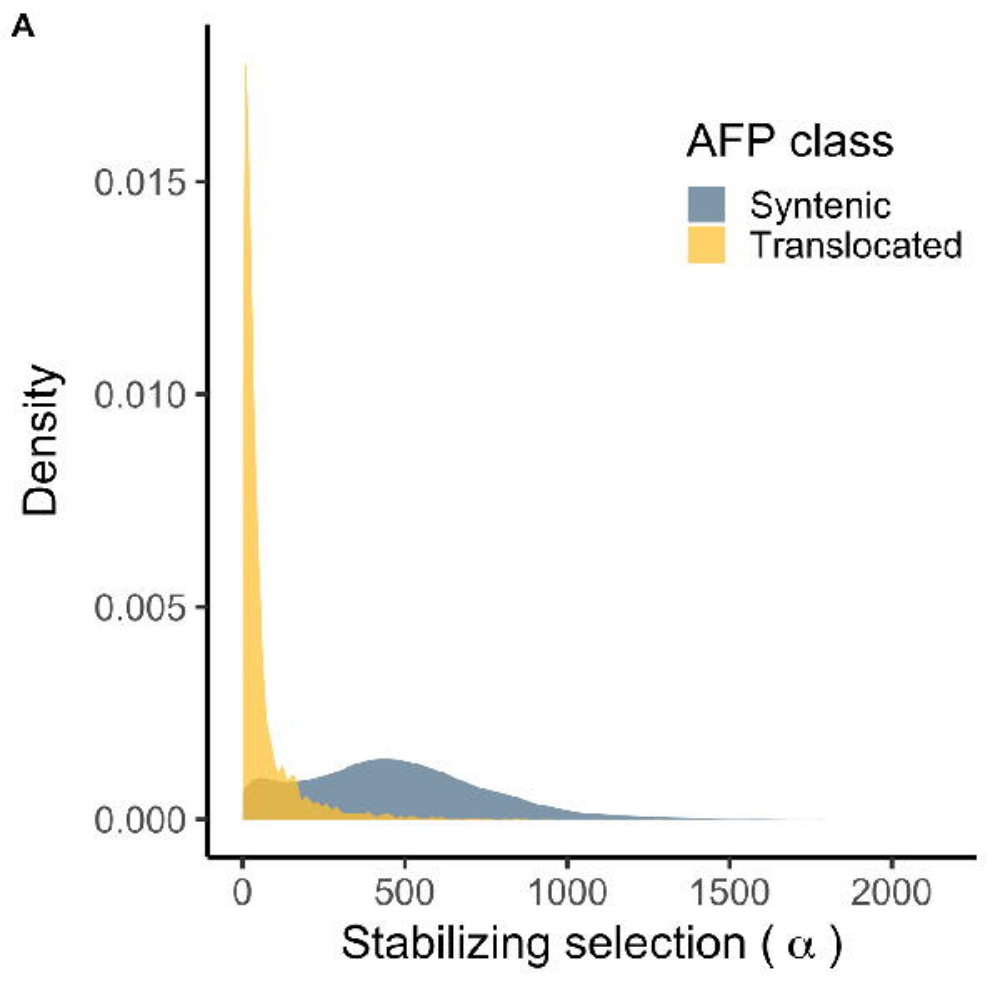
A
AFP class
Syntenic
Translocated
Density
0.015
0.010
0.005
0.000
0
500
1000
1500
2000
Stabilizing selection (α)

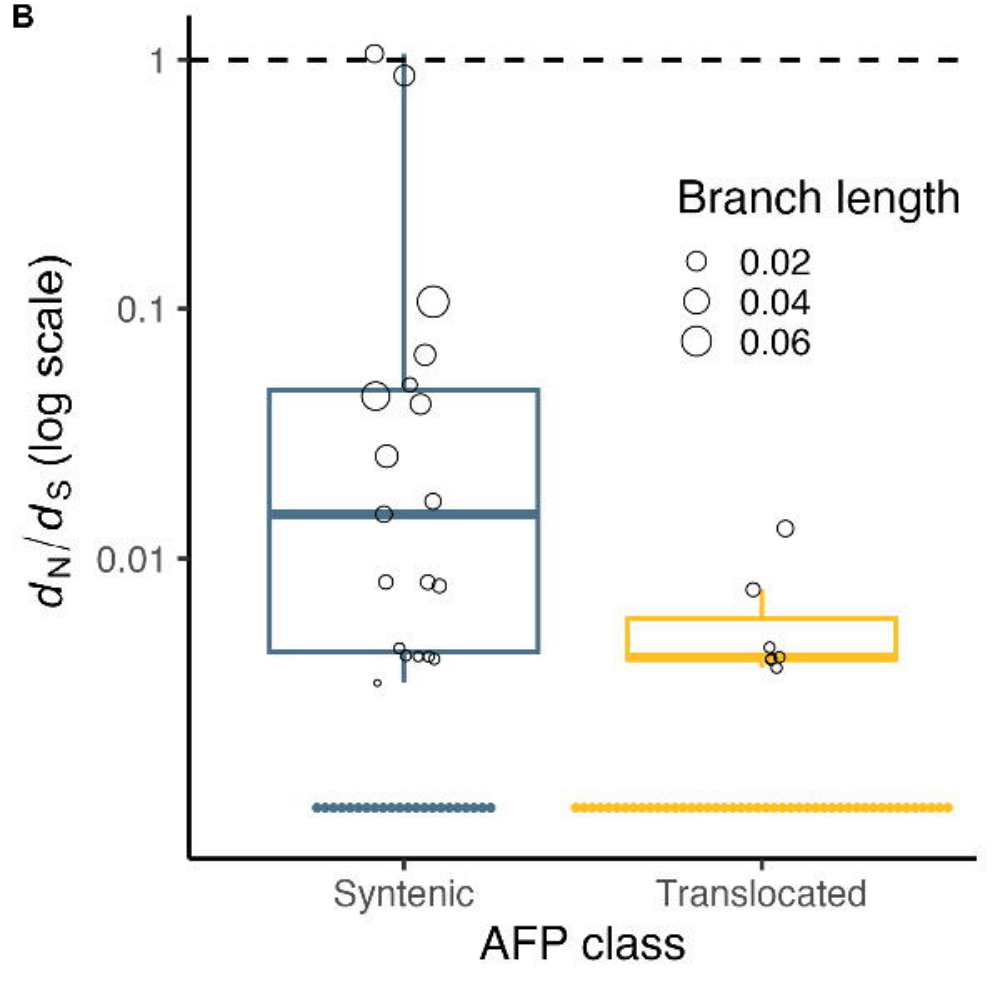
B
Branch length
0.02
0.04
0.06
d_N/d_S (log scale)
1
0.1
0.01
Syntenic
Translocated
AFP class